FLOW ANALYSIS AROUND SPURS OF DIFFERENT PERMEABILITY USING ANSYS FLUENT

A Dissertation submitted in partial fulfillment of the requirement for the Award of degree of

MASTER OF TECHNOLOGY

IN

HYDRAULICS & FLOOD ENGINEERING

BY

SAARTHAK
(ROLL NO. 2K13/HFE/08)

Under the Guidance of

Dr. RAKESH KUMAR

Professor
Department of Civil Engineering
Delhi Technological University
Delhi

DELHI TECHNOLOGICAL UNIVERSITY
(FORMERLY DELHI COLLEGE OF ENGINEERING)
DELHI - 110042
July-2015

CANDIDATE'S DECLARATION

I do hereby certify that the work presented is the report entitled "**Flow Analysis around spurs of different permeability using Ansys Fluent**" in the partial fulfillment of the requirements for the award of the degree of "Master of Technology" in Hydraulics & Flood engineering submitted in the Department of Civil Engineering, Delhi Technological University, is an authentic record of my own work carried out from January 2015 to July 2015 under the supervision of Dr. Rakesh Kumar (Professor), Department of Civil Engineering.

I have not submitted the matter embodied in the report for the award of any other degree or diploma.

Saarthak

Date:29/7/15 (2K13/HFE/08)

CERTIFICATE

This is to certify that above statement made by the candidate is correct to best of my knowledge.

Dr. Rakesh Kumar
(Professor)
Department of Civil Engineering
Delhi Technological University

ACKNOWLEDGEMENT

I take this opportunity to express my profound gratitude and deep regards to Dr. Rakesh Kumar (Professor, Civil Engineering Department, DTU) for his exemplary guidance, monitoring and constant encouragement throughout the course of this project work. The blessing, help and guidance given by him from time to time shall carry me a long way in life on which I am going to embark.

I would also like to thank Dr. Nirendra Dev (Head of Department, Civil Engineering Department, DTU) for extending his support and guidance.

Professors and faculties of the Department of Civil Engineering, DTU, have always extended their full co-operation and help. They have been kind enough to give their opinions on the project matter; I am deeply obliged to them. They have been a source of encouragement and have continuously been supporting me with their knowledge base, during the study. Several of well-wishers extended their help to me directly or indirectly and we are grateful to all of them without whom it would have been impossible for me to carry on my work.

ABSTRACT

Spurs are installed along the river side and are used for various purposes including flow and erosion control and bank protection. The influence factors of spur are largely related to the stream characteristics, hydrologic variables, hydraulic characteristics and local variables. So the analysis considering all the factors becomes difficult. Therefore most of the researches have been focused on the local scour at the tip of the spurs, flow pattern near spurs and separation length. In this study a single spur has been analysed using ANSYS Fluent software. The turbulence model used was standard k-epsilon model for the flow. Four different lengths of spurs were taken i.e. 0.2m, 0.3m, 0.4m, 0.5m and each of five different permeabilities i.e. impermeable, 20%, 40%, 60% and 80%. Three different approach velocities were taken i.e. 0.25m/s, 0.30m/s and 0.40m/s. So in total 60 different combinations of cases were analyzed and compared with the experimental data obtained by Yeo et al. The tip velocities and separation length were compared with the experimental data. Multiple linear regression has been used to see the relationship and correlation between the tip velocities, maximum velocities, permeability of spurs, area ratio of spurs, maximum bed shear stress and separation length. The best permeability of spur that can be used has been found using the results of separation length and maximum bed shear stress.

CONTENTS

LIST OF FIGURES

LIST OF TABLES

LIST OF SYMBOLS

Symbol	Title
A*	Area ratio of spurs
A_g	Lateral projecting area of spur on the channel cross section
A_c	Cross-sectional area of flow in channel
V_{app}	Velocity of approach to spur in m/s
V_{tip}	Tip velocity at spur in m/s
$V_{tip(exp)}$	Tip velocity obtained experimentally in m/s
$V_{tip(num)}$	Tip velocity obtained numerically in m/s
V_{max}	Maximum velocity near spur in m/s
X	distance along the direction of flow from the tip of spur in m
Z	distance across the direction of flow from the tip of the spur in m
τ_m	Maximum bed shear stress in pascals
τ_0	Shear stress of undisturbed approach flow in pascals
τ_m/τ_0	Shear stress amplification
l	Length of spur in m
L	Separation length in m
L_{exp}	Separation length obtained experimentally in m
L_{num}	Separation length obtained numerically in m
B	Width of channel
P	Permeability of spur
R	Correlation coefficient

CHAPTER 1-INTRODUCTION

Spurs, also known as Groynes, are hydraulic structures used in river engineering extending from the bank of the river perpendicularly or at some angle to the watercourse. They are made of gravel, stone, earth, rock, or piles, beginning at the riverbank with a root and ending at the regulation line with a head.

Some of the important functions of Spurs are:-

i. Protection of the river bank from high velocity current by keeping the flow away and towards the channel centre ;
ii. Improving the depth of navigation by contracting the width of channel;
iii. Improving channel alignment by increased sediment deposition near river banks;
iv. Restoration of fish habitats and river ecosystem;

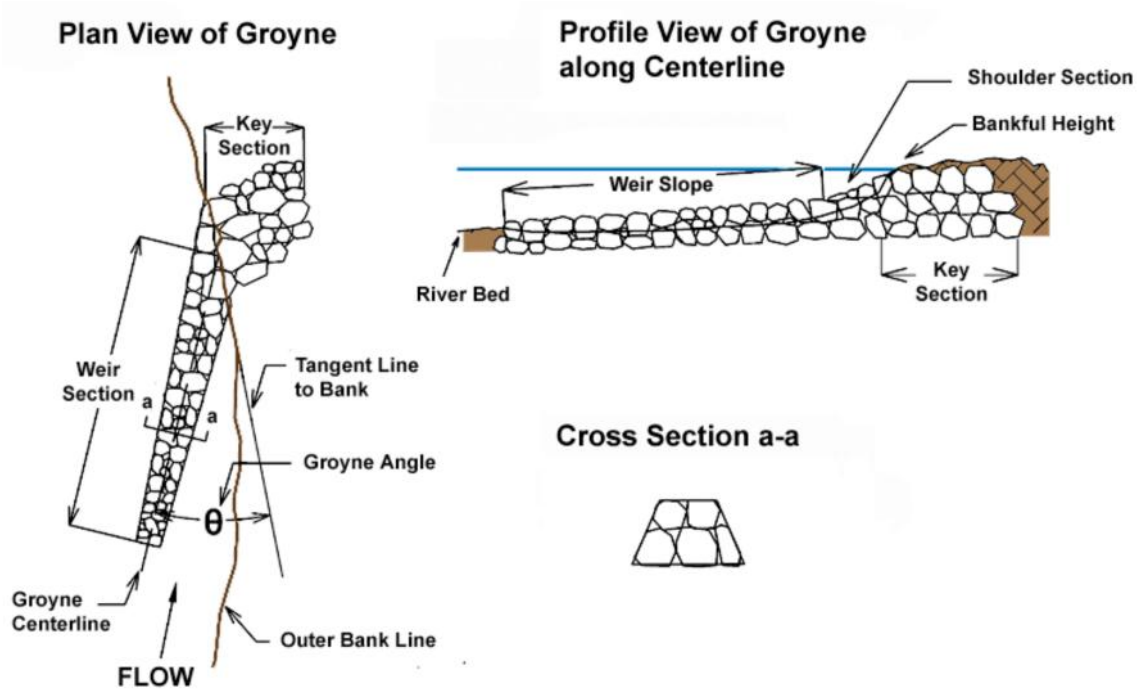

Fig.1.1 Plan, profile, and cross section views of typical spur used for bank protection

1.1 Objective of Dissertation

The objective of this study is:

i. To verify the numerical data obtained from the ANSYS Fluent and compare it to the data obtained from the experiments and thus having good agreement with the experimental data.

ii. To develop a relationship between the tip velocity, approach velocity, permeability of spur and area ratio after comparing the numerical data with the experimental data.

iii. To identify the maximum velocity in the area near the spur and its position from the tip of the spur.

iv. To develop a relationship between maximum bed shear stress, tip velocity, permeability of spur and area ratio.

v. To identify the best permeability of spur based on the results of separation length and maximum bed shear stress.

1.2 Scope of the project

The present study focuses on flow analysis around a single spur of different permeabilities. The study of tip velocity can be used to study scour factor near spur. The separation length can be used in deciding the installation interval in a series of spurs. The maximum bed shear stress can be related to zone of high potential of scouring. The analysis of the shear stress field at the bed of the channel presents a particular interest for studying the sediment transport around a spur dike. The criterion of initial motion of sediment at the bed is estimated using a critical shear threshold. The result of the present study will tell the best permeability of the spur that can be used which gives less bed shear stress and sufficient separation length. ANSYS Fluent has been used throughout the project to analyse the flow around the spur and tip velocities, maximum velocities, separation length and maximum bed shear stress has been calculated. This software contains many models for turbulent flow analysis but here the simplest model has been used to analyse the flow to understand the work easily.

1.3 Types of Spurs

Spurs can be classified into four categories:

1. Material and method of construction:- Permeable or impermeable. Permeable spurs allow water to flow through them and are generally used in rivers with high sediment loads where deposition around spurs is desired. They are also used in milder bends or in rivers with low flow rates. They can be made from timber, bamboo or piles. Impermeable spurs do not allow water to pass through, thus causing the water current to deflect. They are generally used in protecting banks in navigable channels where high depth of flow is required in the centre of channel. They can be made from rocks or gabions.
2. Submergence:- Submerged or emergent. It depends on the water depth. Impermeable spurs are generally designed to be emergent as they experience high scour along their side walls when they are submerged. Permeable spurs are designed submerged as they induce smaller amount of local scour.
3. Action of streamflow:- Attracting, repelling or straight. Attracting spurs point downstream, thus attracting flow towards themselves. They are less effective in bank protection. Straight spurs are at 90^0 to the bank line and they change the direction of flow. Repelling spurs point upstream and repel the flow away from the bank . They are most suited for bank protection.
4. Appearance in plan view:- This includes ‘T-head’, ‘L-head’ , ‘hockey’, ‘inverted hockey’.

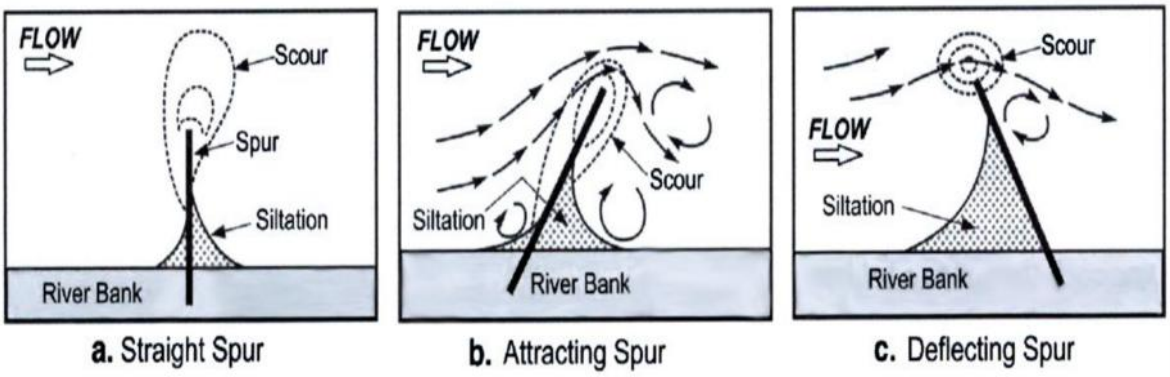

Fig.1.2 Classification of spurs by action on streamflow

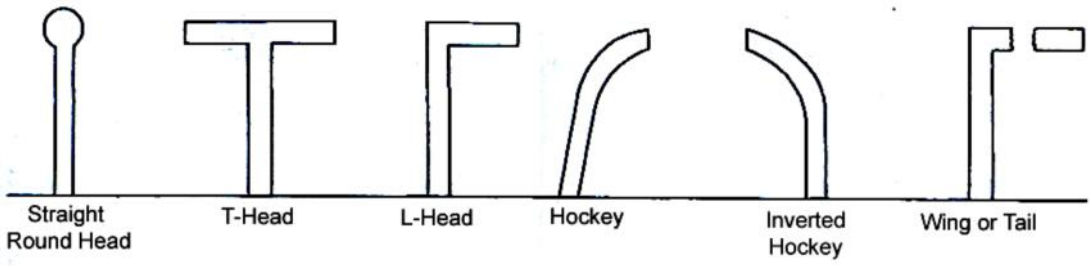

Fig.1.3 Classification of spurs by appearance in plan view

1.4 Design considerations for Spurs

The important considerations for design of spurs are:-

i. Length of spurs:- Its length depends on the location, purpose, spacing, and economics of construction. The length can be established by determining the channel width and depth desired.
ii. Spacing of spurs:- The spacing between spurs is measured at the riverbank between their starting points. It is related to river width, spur length, velocity of flow, angle to the bank, orientation to the flow, bank curvature, and purpose.
iii. Planview shape
iv. Orientation of spurs:- Spurs may be oriented perpendicular to the flow or be inclined either upstream or downstream. Each orientation affects the stream in a different way and results in different deposition of sediment in the vicinity of the spur.
v. Cross-section of spurs
vi. Crest elevation and slope
vii. Construction materials
viii. Scour:- The expected scour depth should be taken into consideration in the determination of the base depth of the spurs.

1.5 Flow near Spurs

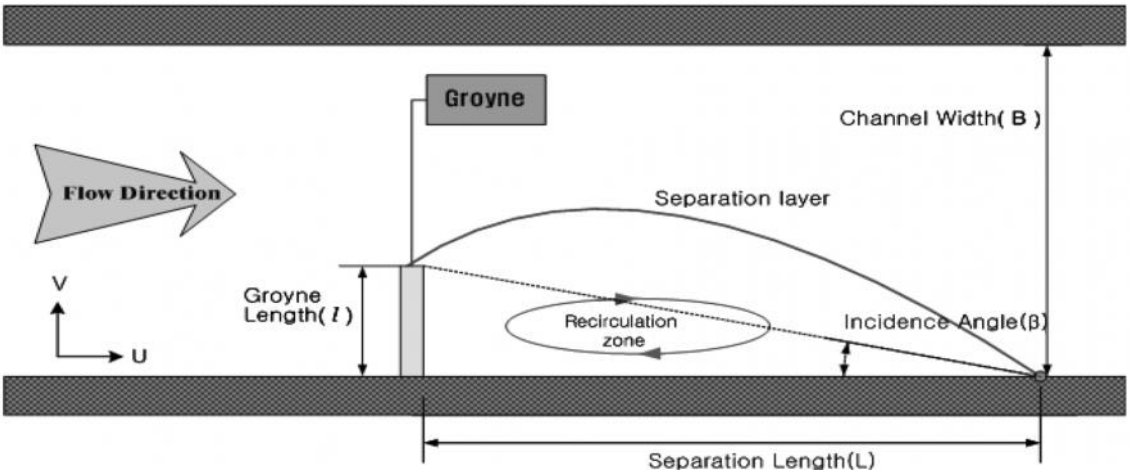

Fig.1.4 Recirculation zone in downstream of spur

There is a common flow pattern after the installation of a spur which is shown in above figure. From the tip of the spur to the opposite channel bank, the flow velocity is increased because of the reduction of the channel width. This is called the main flow zone. The recirculation zone or return flow zone is located at the downstream side of the spur. A velocity difference exists between the main flow zone and the recirculation zone, which leads to the formation of a shear layer between the two zones. In the recirculation zone, a large vortex occurs and two small vortexes also occur upstream and downstream of the large vortex. After a certain distance downstream, this recirculation zone mixes with the main flow to return to the main channel flow pattern. The distance between this returning point and spur installation point is called as separation length. The incident angle at the tip of spur is defined as the angle between the approaching flow direction and the line connecting the separation point and tip of spur.

1.6 Introduction to ANSYS Fluent

Computational Fluid Dynamics (CFD) is a computer based mathematical tool. The emerging interest on the use of CFD based simulation by engineers has long been analysed in various fields of engineering. The basic principle in the application of CFD is to determine fluid flow in-detail by solving a system of non-linear governing equations over the region of interest, after applying specified boundary conditions. The CFD based simulation confides on combined numerical accuracy, modelling precision and computational cost.

ANSYS Fluent is the CFD solver for complex flows. ANSYS Fluent is integrated into the unified ANSYS workbench platform. ANSYS Fluent software gives complete mesh adaptability, including the ability to solve flow problems using unstructured meshes that can be produced about complex geometries. Supported mesh types include quadrilateral, triangular, tetrahedral, hexahedral, pyramid, prism (wedge) and polyhedral. ANSYS Fluent also allows dynamic refinement or coarsening of the mesh based on condition. ANSYS Fluent runs conveniently for all physical models and flow types including steady-state or transient, incompressible or compressible flows , laminar or turbulent flows and Newtonian or non-Newtonian flows. ANSYS Fluent offers powerful solvers for any application: a fully segregated pressure based solver, a coupled pressure based solver with pseudo-transient option, an implicit and an explicit density based solver. The vast majority of open channel flows are turbulent, so ANSYS Fluent software has always placed special priority on providing leading turbulence models to capture the effects of turbulence accurately. Post-processing tools for ANSYS Fluent can be used to make meaningful animations, graphics and reports that make it easy to show fluid dynamics results. Shaded and transparent surfaces, pathlines, vector plots, contour plots, custom field variable definition and scene construction are just some of the post-processing features that are available.

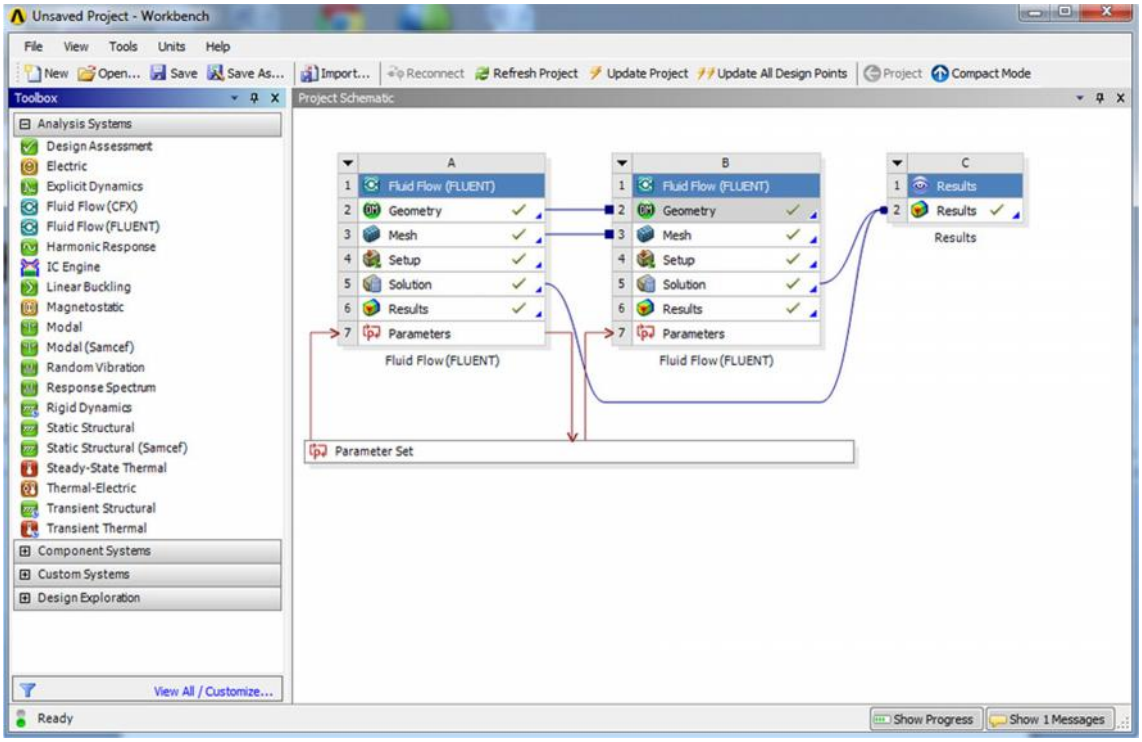

Fig.1.5 Overview of ANSYS Fluent

1.7 Organisation of Dissertation

The report is subdivided into 6 chapters. *Chapter 1* states the importance of the matter and aim of the study. *Chapter 2* presents the review of the literature available on this topic. The methodology and numerical data involved in this dissertation work is discussed in *Chapter 3* and *Chapter 4* respectively. The results and the discussions are enlisted in *Chapter 5*. Finally in *Chapter 6*, conclusions and scope of future work are discussed.

CHAPTER 2-LITERATURE REVIEW

In this dissertation work, various papers are referred and they are enlisted in the bibliography. Many researchers have performed experiments to analyse the flow nature around the spur in various years. Francis et al. [6] performed various experiments in a rectangular flume to study the downstream recirculation zone but they did not measure the velocity. They found that the length of eddy zone is chiefly dependent upon the relative size of the spur, and independent of face angle, form of spur, or sweep angle in the normal range.

Rajaratnam and Nwachukwu [19] performed experimental studies on the structure of turbulent flow near groyne like structures. They analysed the deflected flow using the model of the three dimensional turbulent boundary layer. They used thin plate groynes as well as semi-cylindrical hose groyne for analysis.

Tingsanchali and Maheswaran [24] used 2D depth averaged model to calculate the depth averaged velocity and bottom shear stress distribution near a impermeable groyne. They used hybrid finite difference scheme to solve the transport equations. They used k-ϵ model with a correction factor to measure the velocities and bottom shear stresses.

Ouillon and Dartus [18] performed a 3D numerical simulation of a steady, shallow turbulent flow around a groyne in a rectangular channel. They compared isolines of water depths and mean velocity fields with experimental data. They analysed the results of pressure field, shear stress distribution and turbulence.

Mioduszewski et al. [17] studied the influence of the structure permeability on flow pattern and local scouring process near a groyne. The parameters which leads to scouring were of smaller intensity for permeable groyne than impermeable groyne. Seepage force was not seen in case of permeable structure.

Ettema and Muste [5] performed a series of flume experiments to determine the scale effects in small scale models of flow around a single spur dike placed in a fixed and flat bed channel. The parameters they studied were flow-thawleg alignment(line of maximum streamwise velocity) and area of extent of recirculation zone. They showed

that use of a shear stress parameter as the primary criterion for dynamic similitude influences these parameters.

Uijttewaal [25] performed experiments in physical model of a river reach geometrically scaled to 1:40. Four different types of groynes were tested and all of them were arranged in an array of five identical groyne fields. Flow velocities were measured using PTV. The design of experiment was such that the cross sectional area blocked by the groyne was same in all the experiments. The experimental data were used to understand the physical processes like vortex formation and recirculation zone.

Yeo et al. [27] performed 69 experiments in a flat and fixed open channel with groynes made of acrylic of different permeabilities, relative lengths approach velocities. He changed the permeability of groynes by providing gaps between the acrylic cylinders. The tip velocity of the groyne were measured with the acoustic dopple velocimeter(ADV). The two dimensional velocity field were measured with large scale particle image velocimeter(LSPIV) technique. He suggested an empirical equation for tip velocity in terms of approach velocity and groyne area ratio. He also suggested an empirical equation describing the relationship between the ratio of the separation length to groyne length and Froude number.

Xuelin et al. [23] used large eddy simulations to model the three dimensional flows around a non-submerged spur dike. The finite volume method was used to discretize the Navier-Stokes equations, and the SIMPLEC algorithm was used to solve them. The computational results were in good agreement with experimental results.

Ho et al. [11] performed numerical modelling in FLOW-3D software for single groyne in a rectangular flume to investigate flow pattern changes and to find the best performing installation interval. He developed numerical model for the experiments performed by Yeo et al [27].

McCoy et al. [16] performed a Large eddy simulation(LES) on the groyne field in a straight open channel. The mean velocity at the free surface was found to be in good agreement with the experimental results. The bed shear stress was found to be more in the region close to downstream of the groyne.

Kang et al. [13] performed hydraulic experiments in fixed and movable beds to examine the flow pattern, bed change and scour depth and hole around a groyne. Both permeable

and impermeable groynes were used for testing. The maximum scour depth for each groyne type moved along a linearly downward path with increasing permeability. The scour depth was decreasing with increase in permeability. The maximum scour depth was greatest with perpendicular groyne. The scour area was much larger for impermeable groyne than permeable groyne.

Duan [4] experimentally studied the three dimensional turbulent flow field around a spur dike in a fixed bed open channel using a microacoustic dopple velocimeter. Mean and turbulence characteristics were evaluated upstream and downstream of the spur. The maximum bed shear stresses estimated using Reynolds stresses were about three times the mean bed shear stresses of the incoming flow.

Safarzadeh et al. [20] performed experimental measurements to investigate the head shape effects on bed shear stress distribution around single straight and T-shape groynes. Distribution of shear stress was more uniform downstream of the T-shape groyne.

Yazdi et al. [26] used Fluent software to study the flow patterns around a single spur dike. He used standard k-ω turbulence model with VOF method to get the results. By comparing the reults with experimental data, the model was found to produce flow around a spur dike with sufficient accuracy.

Baba et al. [3] performed some experimental studies were carried out using the LSPIV technique and an electromagnetic velocimeter. The velocity distributions and longitudinal length of the recirculation area were calculated. Both permeable and impermeable dikes were used for experiments. It was found that permeable spur dike was better alternative than impermeable spur dike in terms of morphodynamics around the spur dike.

Yossef and Vriend [28] performed experiments on a fixed bed flume for a schematized river reach with groynes on one side to study the dynamics of the flow near groynes. The flume was made to a geometrical scale of 1:40 based on the dimensions of the river waal. Large scale velocity fluctuations were found in all the test cases. The submerged groynes showed different turbulence pattern from the emerged groynes. The sediment transport rate was found to be proportional to the velocity to a certain power.

Shahrokhi and Sarveram [21] used Flow-3D software to provide a numerical model of groyne surrounding flow by using large eddy turbulence model while studying the effects of these factors on separation length and width of separation region behind a groyne by applying various installation angles, groyne lengths and flow velocities. The separation region length and width were maximum for angle of installation of 105^0 .

Hakimzadeh et al. [9] studied the effect of structural slope of model groynes on scour reduction. Total 8 tests were performed with different lateral slopes of groynes. The experimental results showed that the maximum scour depth at the head of groynes was reduced by 22% by reducing the structural slopes of groynes. The transported sediments volume for mildest lateral slope groyne reduced significantly when compared with rectangular groyne.

Ghani et al. [8] used Fluent software to validate the data of Zhang et al.(2009)[31]. The numerical results were in good agrrement with the experimental results.

Mansoori et al. [15] investigated three-dimensional flow structure around two simple series of groynes with different shapes of head using a numerical model known as SSIIM. Two case studies were considered: a simple series of straight groynes and a simple series of groynes with T-shape head. A brief discussion about the physics of flow was done in order to compare the performance of a series of T-shape groynes with that of straight ones based on the primary objectives of the designs of the groynes.

Acharya et al. [1] presented a 3D numerical simulation of turbulent flow field around a series of three experimental dikes in a flat and scoured bed surface using Flow-3d software. They used three different numerical models in Flow-3d to compare the results from the experimental data.

Ghaidarbandi et al. [7] studied the effects of the cross shore and groyne wall slopes on flow parameters around an impermeable groyne using Fluent software. They used k-ϵ RNG model to analyse the flow. The numerical model results were in good agreement with the experimental work and they revealed that by increasing the cross shore bed slope magnitude of maximum velocity and bed shear stress decreased. These valued decreased further as the structural slope was reduced.

Zhang et al. [31] presented an experimental study on the bed variation characteristics and the corresponding flow structure around different types of groynes in sediment

mixtures. Impermeable and permeable spur dykes were combined in various ways and their hydro-morphological implications were investigated.

Shamloo and Pirzadeh [22] used Fluent software to validate the experimental results of Yeo et al. [27]. They used Reynolds stress turbulence model(RSM) in Fluent software to estimate the turbulent flow field. The numerical results showed satisfying agreement with the experimental data.

Karami et al. [14] investigated scour phenomenon around a series of impermeable, non-submerged spur dikes with both experimental and numerical methods. The experiments were conducted with different states of flow intensity. For numerical simulation SSIIM 2.0 was used to compute the data. They used RNG k-ϵ turbulence model and finally the experimental and numerical data were compared.

Asayama and Kadota [2] conducted field investigation to measure the sizes of groynes as well as bed morphology around the groynes. A Particle tracking velocimetry(PTV), 3D flow numerical analysis of flow and bed variation around the groynes were performed. They proposed a simple arrangement of river structure for stable bed morphology.

Kafle [12] presented a numerical model to simulate two- dimensional flow near a spur-dike. The CFD program named Nays 2D was used to simulate the flow field in a fixed flat bed around the spur dike introduced into the flow at 90° to the stream-wise direction. Several turbulence closurer models k-ε model, zero equation model and constant eddy viscosity model were applied and compared in order to achieve the best result. The simulated results were compared with existing experimental and computed data.

In this dissertation work, the experimental data of Yeo et al. [27] has been used for comparison with the numerical data in ANSYS Fluent. Standard k-ε model has been used for analysis. The data given by Yeo et al. [27] was used because it had all the necessary data required for input in ANSYS Fluent and all the experimental data were given properly for the comparison with the numerical data.

CHAPTER 3-METHODOLOGY

3.1 Overview of Experiments

The tip velocity at spur was measured by ADV (Acoustic Doppler Velocimeter, Nortek AS) and sampling frequency was 25 Hz. LSPIV technique was applied for the recirculation zone. The applied LIPIV used Digital Video Camera (DTR-TRV900, Sony Co.) and popped rice for seeding and CACTUS 3.1(IIT Co.) as an analysing program. The flume was 40 m long (including transparent grass of 30 m) 2.0 m wide and 0.65 m deep. It had water supply tank with weir of 1.2 m that supplied depth of 0.012~0.4 cms. The model of spur was made of acrylic. In case of permeable type, permeability was given by changing the interval of the acrylic cylinders with 2 cm diameter. Fig.3.1 and Fig.3.2 show the measuring instruments and facilities.

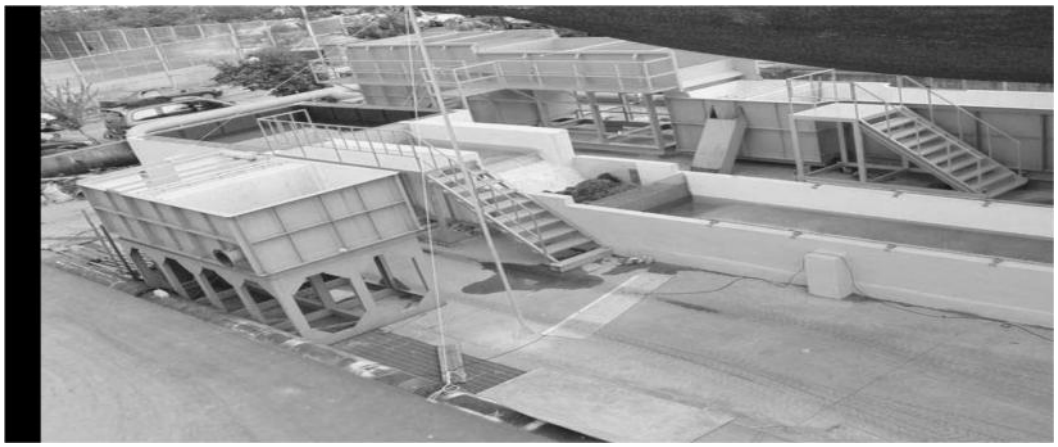

Fig.3.1 Water supply tank

Fig.3.2 Setting in the straight channel

Total 60 experiments were performed in the channel. The experiments were divided in 4 cases as the ratio of spur length to channel width, 0.10, 0.15, 0.20, and 0.25, and 5 cases of permeability, 0% (impermeable), 20%, 40%, 60%, and 80%. Three different tip velocities were considered in each case i.e 0.25, 0.30 and 0.40 m/s. The tip velocity of the spur was measured at the middle layer (60% of the water depth) by using ADV (Fig.3.3). The computed data of ADV were time averaged for every minute. The depth of flow was 0.15m in every case. The velocity field was measured by using LSPIV technique. The obtained images were converted into the velocity field by using CACTUS 3.1.

Fig.3.3 The Tip Velocity measurement by ADV

Fig.3.4 shows an example of the application. Since the object of this study was analysis of the effect of the spur design factors the LSPIV technique was found very useful.

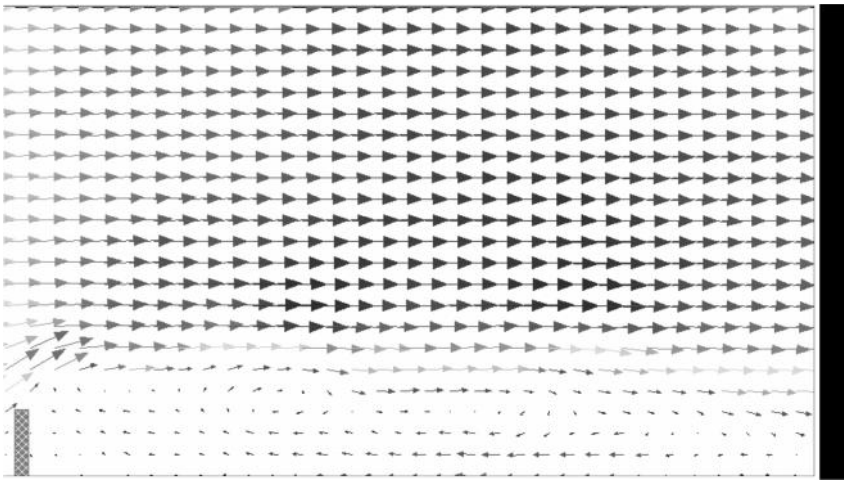

Fig.3.4 Velocity vector field from LSPIV method

3.2 Numerical method

The experiment described above has been analysed in ANSYS FLUENT. The process of the numerical simulation of fluid flow generally involves three steps:

(a) Pre-Processing

- Geometry set-up and Discretization of domain
- Defining the flow condition (e.g laminar, turbulent etc.)
- Defining the boundary condition and initial condition

(b) Solver

- The equation emphasizes over and over till desirable level of accuracy is attained.

(c) Post processing

- Results are analysed.

3.2.1 Geometry setup

ANSYS Workbench has its own geometry making software embedded in it. But due to some complex geometries, the models were made in AUTOCAD 2013 and then exported in the ANSYS. Total 20 geometries were made in AUTOCAD 2013 of different spur lengths and permeabilities. The length of the channel was taken to be 10m only to save the extra time for calculation. The width and height of the channel were kept the same as of the experiments. All the geometries have been labelled according to the following table.

Table 3.1 : Nomenclature of geometries

Length of spur in m	Symbol used
0.2	L1
0.3	L2
0.4	L3
0.5	L4

Permeability of spur(%)	Symbol used
0	P1
20	P2
40	P3
60	P4
80	P5

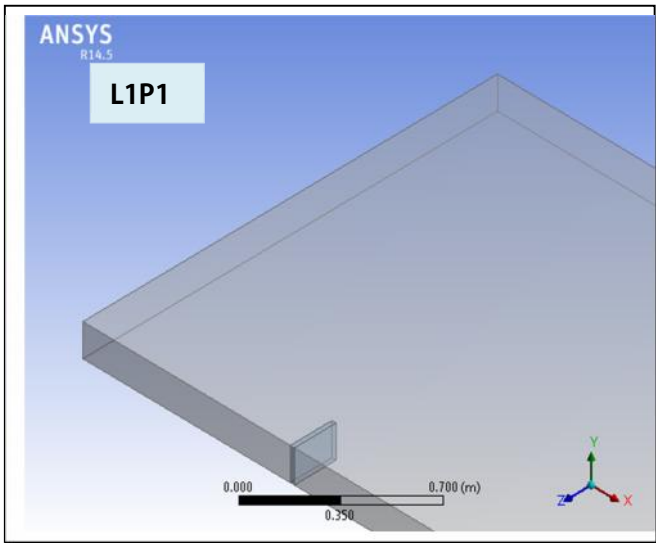

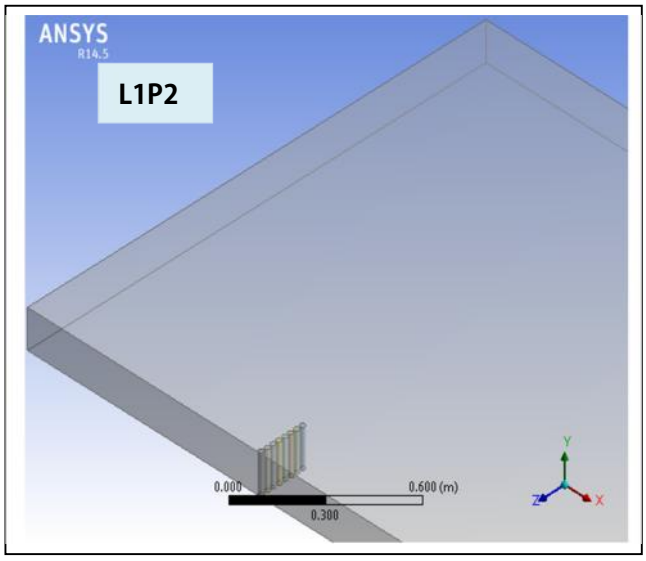

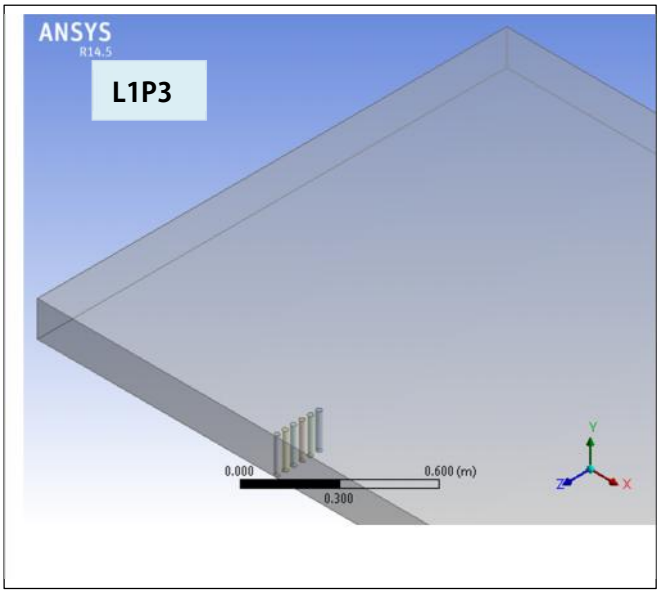

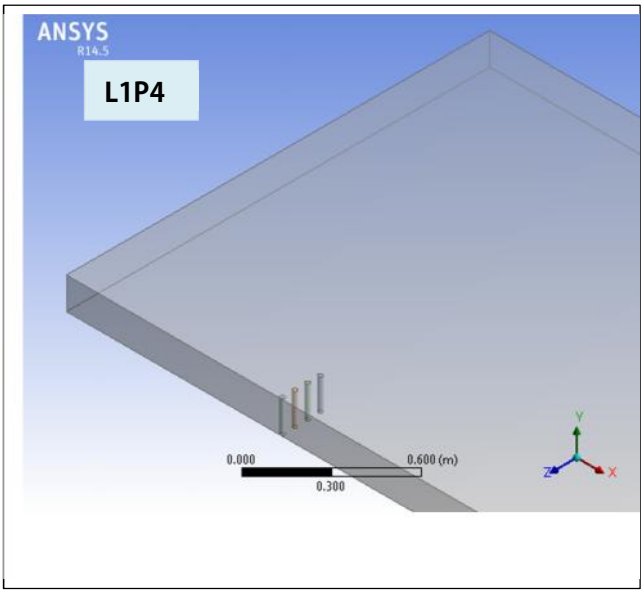

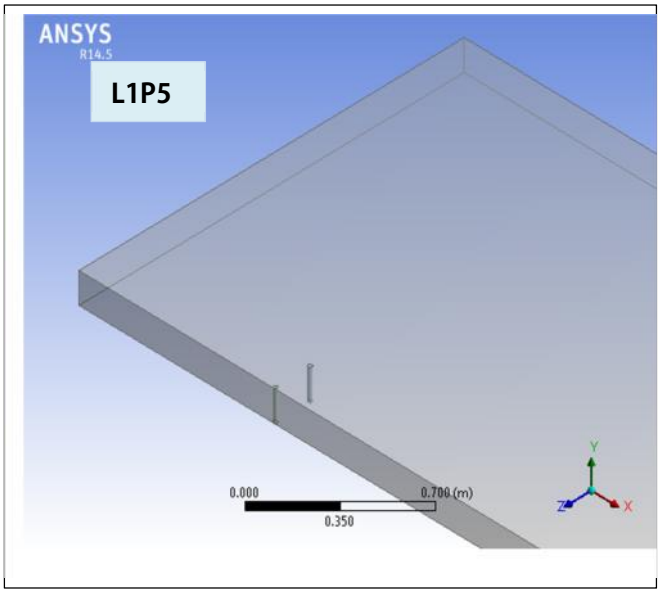

Fig.3.5 Spurs of length 0.2m of different permeabilities

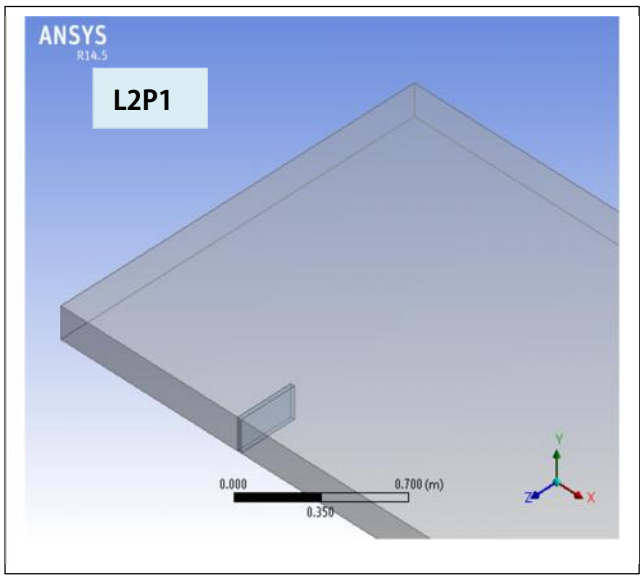

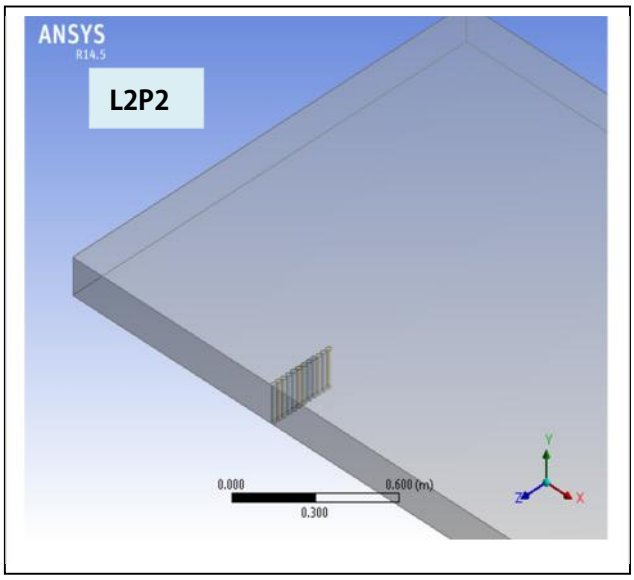

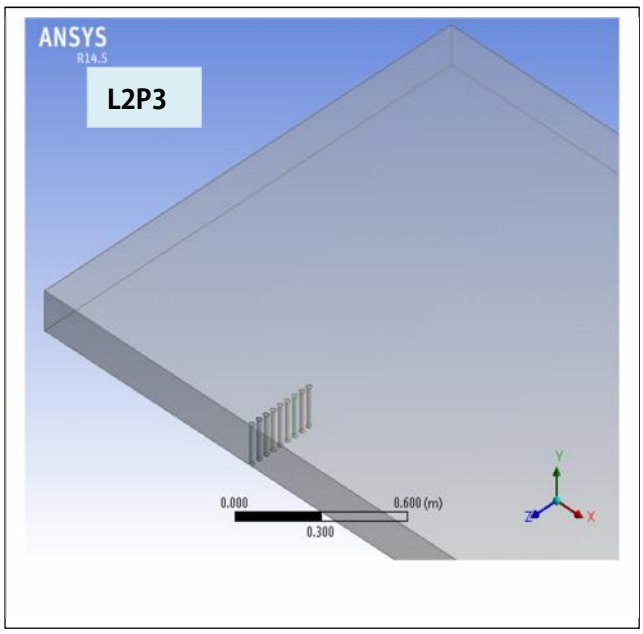

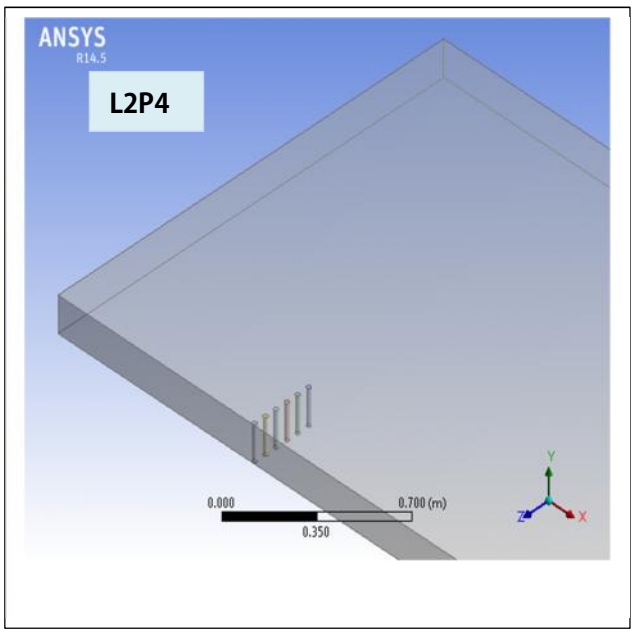

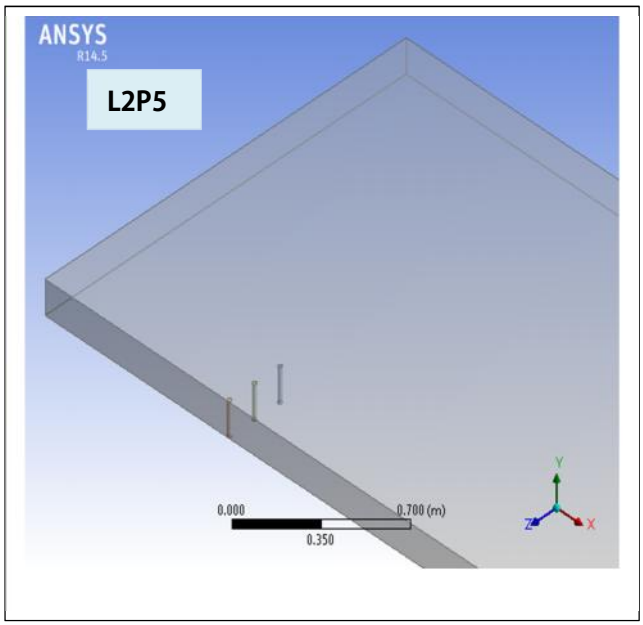

Fig.3.6 Spurs of length 0.3m of different permeabilities

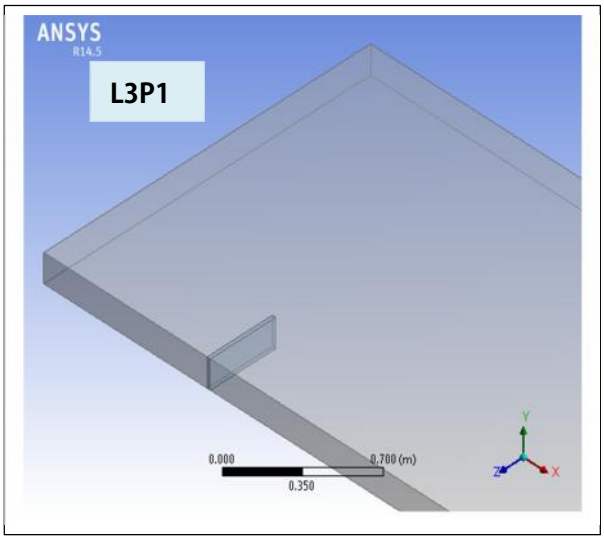

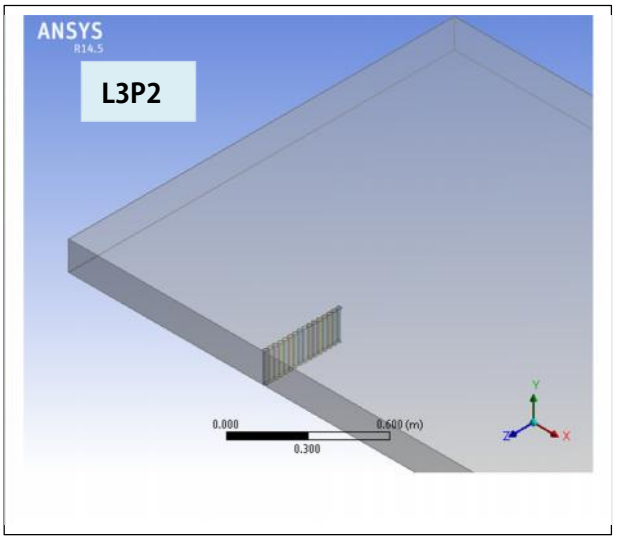

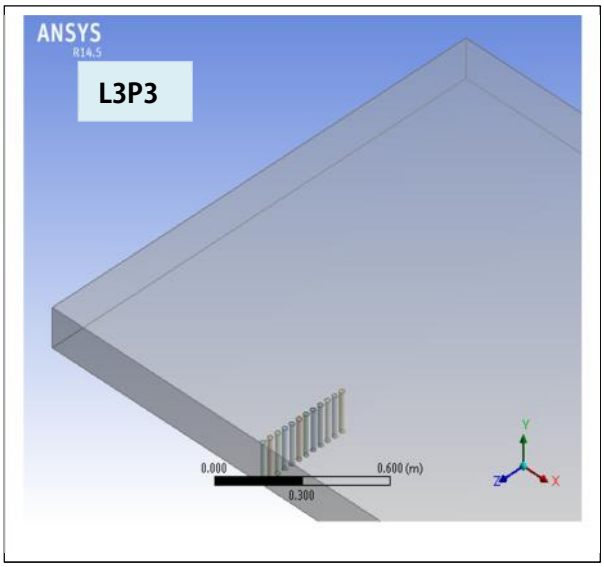

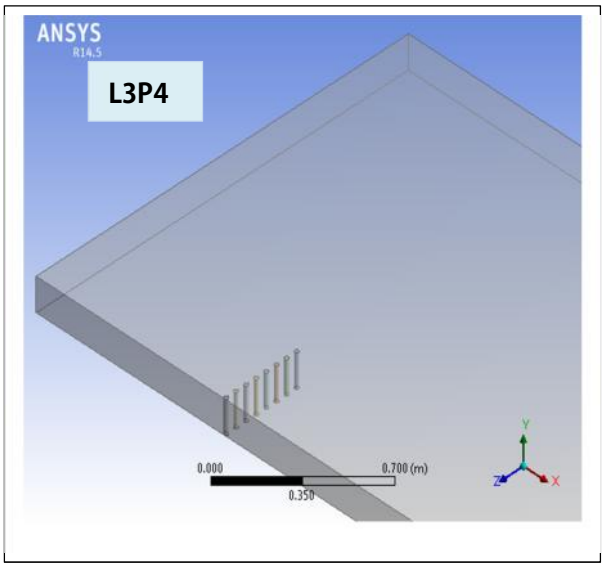

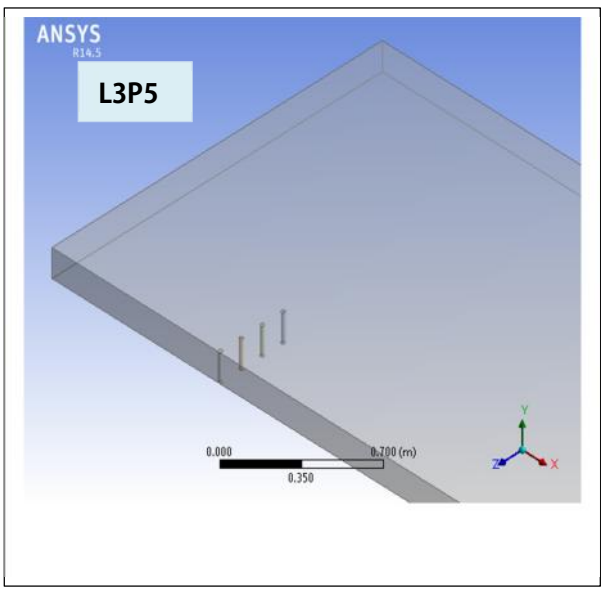

Fig.3.7 Spurs of length 0.4m of different permeabilities

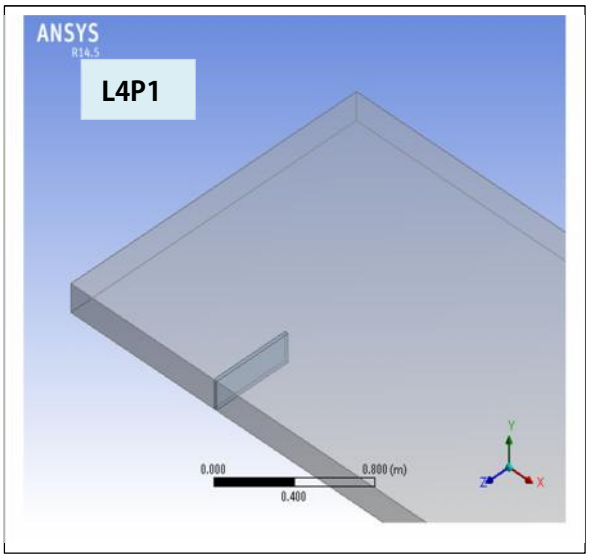

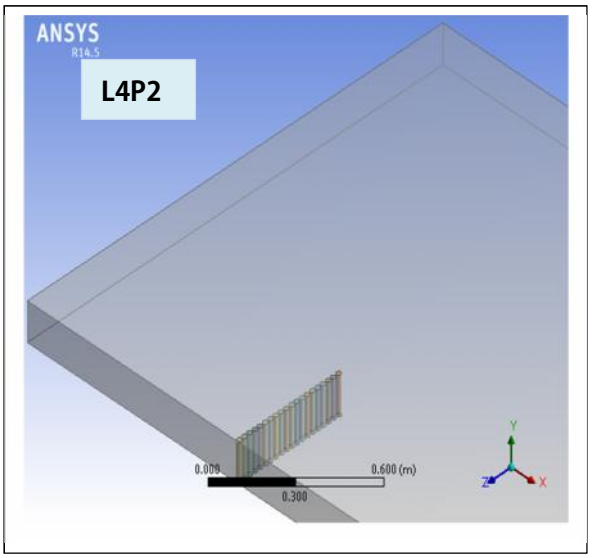

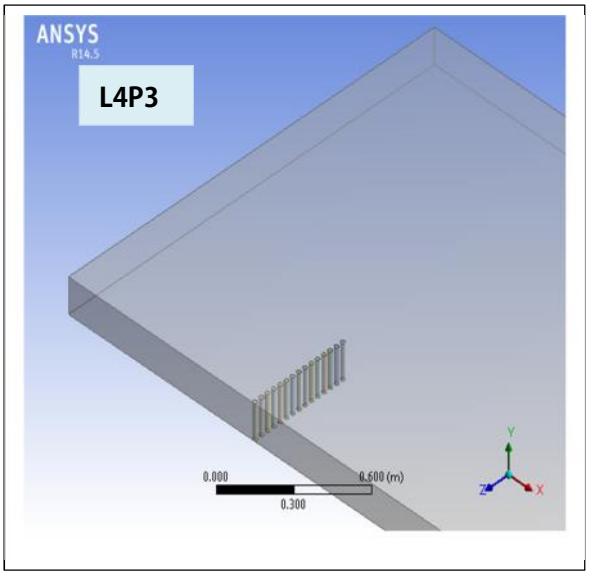

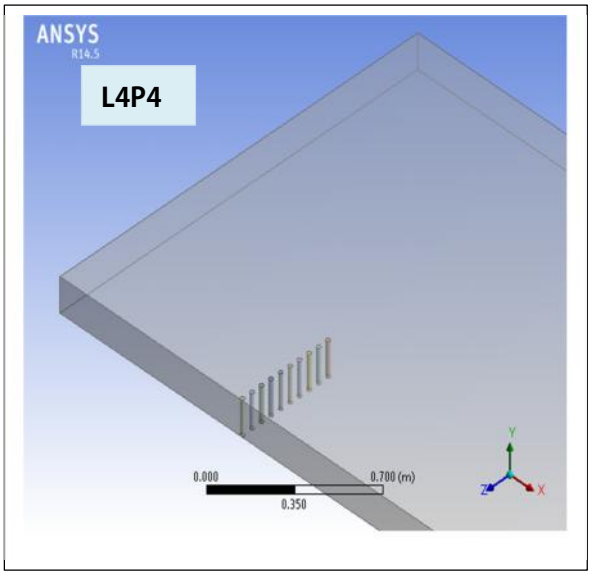

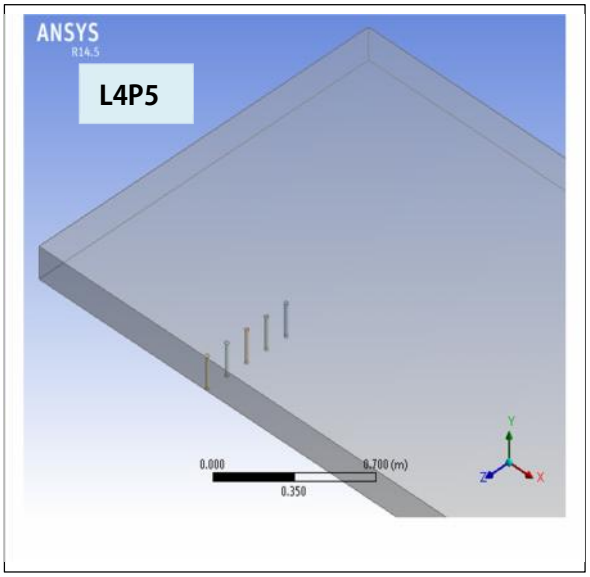

Fig.3.8 Spurs of length 0.5m of different permeabilities

3.2.2 Meshing

ANSYS workbench has its own meshing software. The meshing for permeable and impermeable spurs are different. The meshing elements in the impermeable models are of rectangle shape while in the permeable models are of tetrahedron shape.

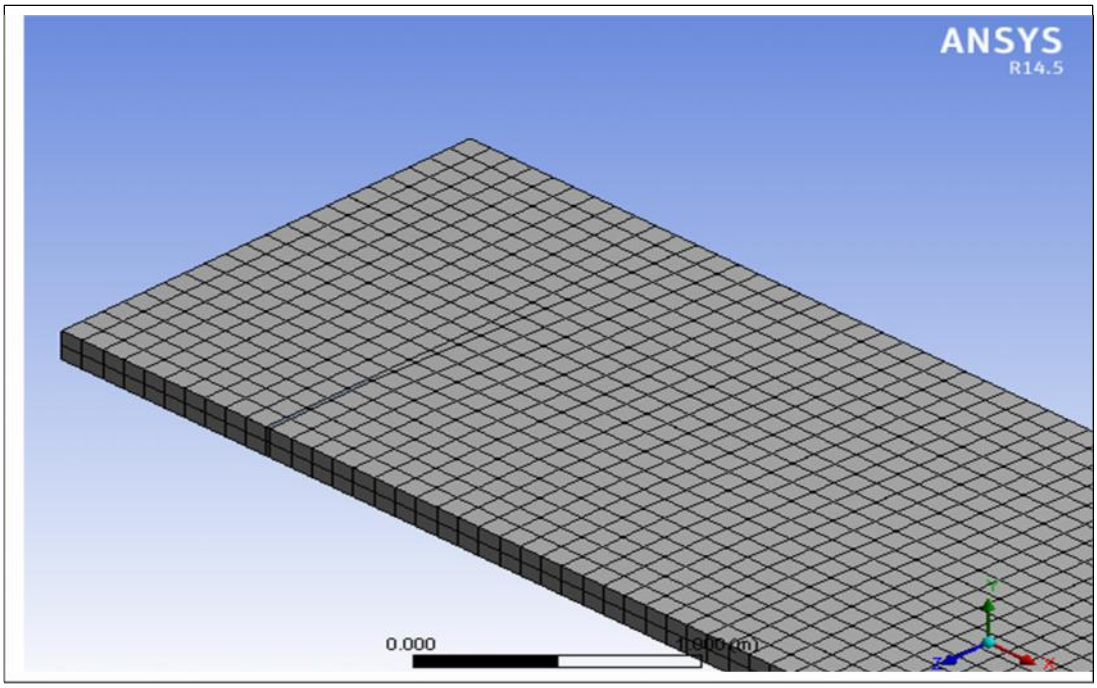

Fig.3.9 Meshing of channel with impermeable spur

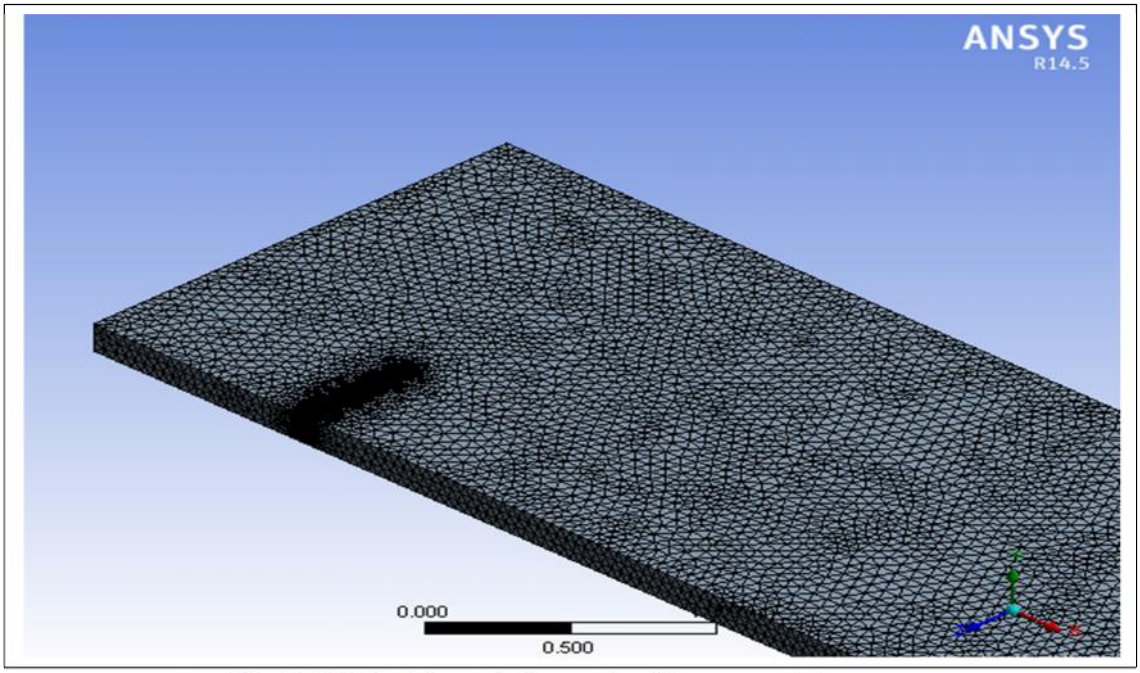

Fig.3.10 Meshing of channel with permeable spur

3.3.3 Fluent setup

The first step in this is to define gravity in –ve y direction. The flow occurs along the x direction. Then next step is to select the type of model to be used in the analysis. Here we have used standard k-epsilon model for the analysis. Some of the models used in fluent are shown below in Fig.3.13.

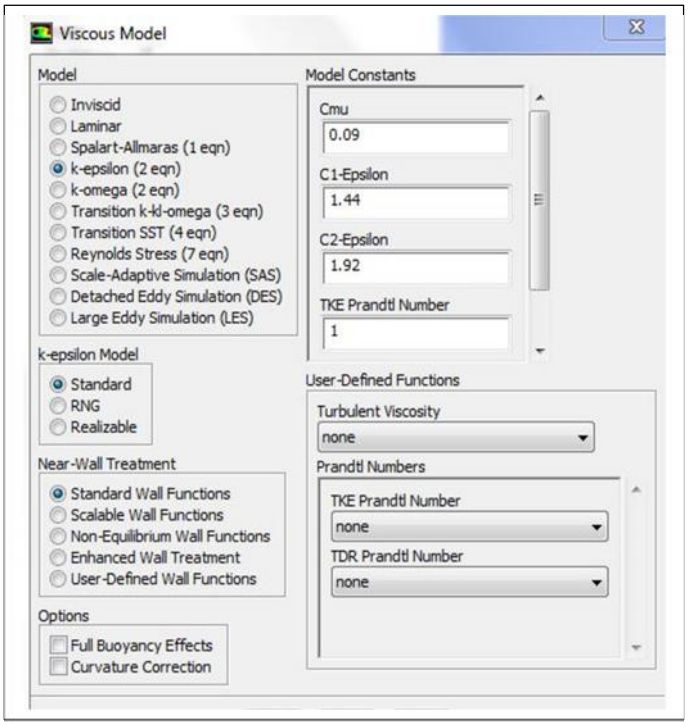

Fig3.11 Various models in Fluent

Standard k-ε model: It is based on model transport equations for the turbulence kinetic energy(k) and its dissipation rate(ε). The model transport equation for k is derived from the exact equation and the model transport equation for ϵ is obtained using physical reasoning. The assumption while deriving k-ϵ model is that the flow is fully turbulent and the effects of molecular viscosity are negligible. The turbulence kinetic energy(k) and its dissipation rate(ε) are obtained from the following transport equations:

$$\frac{\partial}{\partial t}(\rho k) + \frac{\partial}{\partial t}(\rho k u_i) = \frac{\partial}{\partial x_j}\left|\left(\mu + \frac{\mu_t}{\sigma_k}\right)\frac{\partial k}{\partial x_j}\right| + G_k + G_b - \rho\varepsilon - Y_M + S_k \quad \text{.....Eq.3.1}$$

and

$$\frac{\partial}{\partial t}(\rho \varepsilon) + \frac{\partial}{\partial t}(\rho \varepsilon u_i) = \frac{\partial}{\partial x_j}\left|\left(\mu + \frac{\mu_t}{\sigma_\varepsilon}\right)\frac{\partial k}{\partial x_j}\right| + C_{1\varepsilon}\frac{\varepsilon}{k}(G_k + C_{3\varepsilon}G_b) - C_{2\varepsilon}\rho\frac{\varepsilon^2}{k} + S_\varepsilon$$

.....Eq.3.2

In these equations, G_k represents the generation of turbulence kinetic energy due to the mean velocity gradients, G_b is the generation of turbulence kinetic energy due to buoyancy. Y_M represents the contribution of the fluctuating dilatation in compressible turbulence to the overall dissipation rate. $C_{1\varepsilon}, C_{2\varepsilon}$ and $C_{3\varepsilon}$ are constants. σ_k and σ_ε are the turbulent Prandtl numbers for k and ε respectively. S_k and S_ε are user-defined source terms.

The turbulent (or eddy) viscosity, μ_t, is computed by combining k and ε as :

$$\mu_t = \rho C_\mu \frac{k^2}{\varepsilon} \text{.....Eq.3.3}$$

Where C_μ is a constant.

The model constants $C_{1\varepsilon}, C_{2\varepsilon}$, $C_{3\varepsilon}$, σ_k and σ_ε have the following default values

$$C_{1\varepsilon} = 1.44,, C_{2\varepsilon} = 1.92, C_\mu = 0.09, \sigma_k = 1.0, \sigma_\varepsilon = 1.3$$

These default values have been determined from experiments for fundamental turbulent flows including frequently encountered shear flows like boundary layers, mixing layers and jets as well as for decaying isotropic grid turbulence. They have been found to work fairly well for a wide range of wall-bounded and free shear flows.

Materials: Next step in Fluent is to define materials. The spur was made of acrylic (mass density = 1180 kg/m^3). The cell zone condition for the spur has to solid and for model space is liquid.

Boundary conditions: the boundary conditions are as follows;

Inlet- the inlet was taken as velocity-inlet.

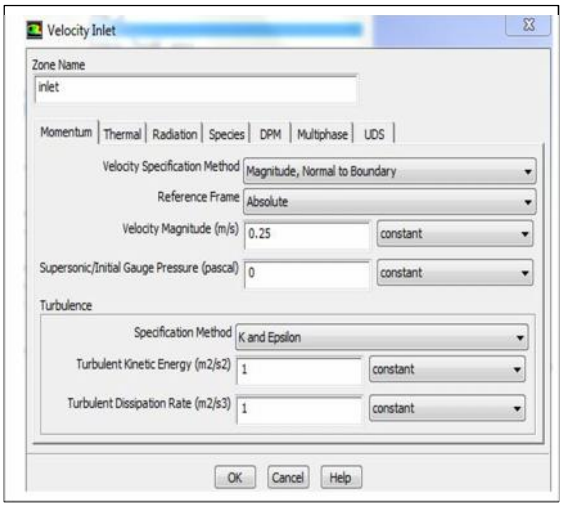

Fig.3.12 Velocity inlet window in Fluent

Outlet- the outlet was taken as outflow with flow rate weighing equal to 1.

Free surface- it was taken as symmetry condition.

Bed and side walls- The channel bed,side walls, and spur surfaces were all set to non-slip surfaces. All surfaces were considered to be hydrodynamically smooth, including the bottom bed.

Solution: next step is to initialize the solution. Then no. of iterations are set to 1000 and the solution is calculated until it is converged. It is necessary for the solution to get converged. The no. of iterations required were always less than 1000. The finer the mesh, the more time it takes to calculate the solution. After the analysis, the results can be viewed under the CFX-POST which is embedded in ANSYS workbench.

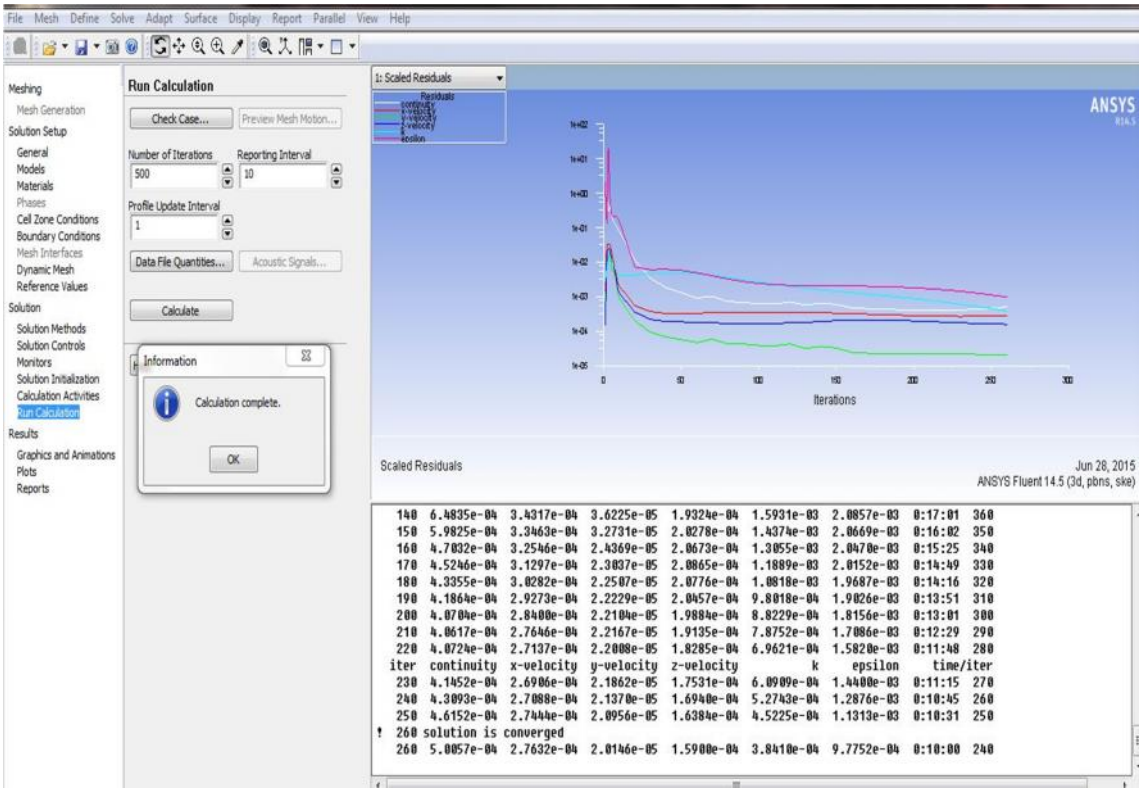

Fig.3.13 Window in Fluent after solution convergence

CHAPTER 4 - NUMERICAL DATA

This chapter contains the data obtained from the Fluent. Total 60 cases were run for spurs of different length, permeability and approach velocity as performed in experiments by Yeo et al.[27]. They assumed that the flow is fully developed at a high Reynolds number and therefore its effect can be ignored.

4.1 Software output

The following table contains the values of tip velocity obtained from the experiments and from the Fluent software. The tip velocity was measured at the middle layer (60% of the water depth).

Here V_{app}= Velocity of approach to spur in m/s, $V_{tip(exp)}$= tip velocity at the spur obtained experimentally in m/s, $V_{tip(num)}$= tip velocity at the spur obtained numerically in m/s, A*=spur area ratio

Table 4.1 : Values of tip velocities in m/s

S.No.	Spur	A*	V_{app}	$V_{tip(exp)}$	$V_{tip(exp)}/ V_{app}$	$V_{tip(num)}$	$V_{tip(num)}/ V_{app}$
1	L1P1	0.111	0.25	0.31	1.24	0.3	1.2
2	L2P1	0.176	0.25	0.35	1.4	0.337	1.348
3	L3P1	0.25	0.25	0.39	1.56	0.386	1.544
4	L4P1	0.33	0.25	0.42	1.68	0.451	1.804
5	L1P2	0.086	0.25	0.31	1.24	0.281	1.124
6	L2P2	0.136	0.25	0.33	1.32	0.303	1.212
7	L3P2	0.19	0.25	0.34	1.36	0.334	1.336
8	L4P2	0.25	0.25	0.36	1.44	0.376	1.504
9	L1P3	0.063	0.25	0.3	1.2	0.278	1.112
10	L2P3	0.098	0.25	0.32	1.28	0.297	1.188
11	L3P3	0.136	0.25	0.32	1.28	0.322	1.288
12	L4P3	0.176	0.25	0.33	1.32	0.352	1.408
13	L1P4	0.041	0.25	0.29	1.16	0.272	1.088
14	L2P4	0.063	0.25	0.3	1.2	0.285	1.14
15	L3P4	0.086	0.25	0.29	1.16	0.303	1.212

S.No.	Spur	A*	V_{app}	$V_{tip(exp)}$	$V_{tip(exp)}/ V_{app}$	$V_{tip(num)}$	$V_{tip(num)}/ V_{app}$
16	L4P4	0.111	0.25	0.29	1.16	0.323	1.292
17	L1P5	0.02	0.25	0.28	1.12	0.263	1.052
18	L2P5	0.03	0.25	0.28	1.12	0.271	1.084
19	L3P5	0.041	0.25	0.27	1.08	0.28	1.12
20	L4P5	0.052	0.25	0.27	1.08	0.289	1.156
21	L1P1	0.111	0.3	0.35	1.17	0.36	1.200
22	L2P1	0.176	0.3	0.39	1.30	0.405	1.350
23	L3P1	0.25	0.3	0.43	1.43	0.463	1.543
24	L4P1	0.33	0.3	0.47	1.57	0.541	1.803
25	L1P2	0.086	0.3	0.35	1.17	0.335	1.117
26	L2P2	0.136	0.3	0.36	1.20	0.361	1.203
27	L3P2	0.19	0.3	0.39	1.30	0.395	1.317
28	L4P2	0.25	0.3	0.42	1.40	0.441	1.470
29	L1P3	0.063	0.3	0.33	1.10	0.332	1.107
30	L2P3	0.098	0.3	0.35	1.17	0.353	1.177
31	L3P3	0.136	0.3	0.36	1.20	0.38	1.267
32	L4P3	0.176	0.3	0.38	1.27	0.413	1.377
33	L1P4	0.041	0.3	0.32	1.07	0.325	1.083
34	L2P4	0.063	0.3	0.33	1.10	0.339	1.130
35	L3P4	0.086	0.3	0.33	1.10	0.358	1.193
36	L4P4	0.111	0.3	0.34	1.13	0.379	1.263
37	L1P5	0.02	0.3	0.31	1.03	0.315	1.050
38	L2P5	0.03	0.3	0.32	1.07	0.323	1.077
39	L3P5	0.041	0.3	0.31	1.03	0.332	1.107
40	L4P5	0.052	0.3	0.31	1.03	0.342	1.140
41	L1P1	0.111	0.4	0.5	1.25	0.481	1.203
42	L2P1	0.176	0.4	0.56	1.4	0.541	1.353
43	L3P1	0.25	0.4	0.61	1.525	0.618	1.545
44	L4P1	0.33	0.4	0.66	1.65	0.722	1.805
45	L1P2	0.086	0.4	0.48	1.2	0.445	1.113
46	L2P2	0.136	0.4	0.51	1.275	0.476	1.190
47	L3P2	0.19	0.4	0.54	1.35	0.52	1.300

S.No.	Spur	A*	V_{app}	$V_{tip(exp)}$	$V_{tip(exp)}/ V_{app}$	$V_{tip(num)}$	$V_{tip(num)}/ V_{app}$
48	L4P2	0.25	0.4	0.58	1.45	0.578	1.445
49	L1P3	0.063	0.4	0.46	1.15	0.439	1.098
50	L2P3	0.098	0.4	0.48	1.2	0.464	1.160
51	L3P3	0.136	0.4	0.5	1.25	0.496	1.240
52	L4P3	0.176	0.4	0.52	1.3	0.534	1.335
53	L1P4	0.041	0.4	0.46	1.15	0.43	1.075
54	L2P4	0.063	0.4	0.46	1.15	0.445	1.113
55	L3P4	0.086	0.4	0.48	1.2	0.467	1.168
56	L4P4	0.111	0.4	0.47	1.175	0.489	1.223
57	L1P5	0.02	0.4	0.44	1.1	0.419	1.048
58	L2P5	0.03	0.4	0.45	1.125	0.425	1.063
59	L3P5	0.041	0.4	0.45	1.125	0.436	1.090
60	L4P5	0.052	0.4	0.44	1.1	0.446	1.115

The following table contains the values of maximum velocity obtained numerically and distance of point of maximum velocity from the tip of the spur.

Here V_{max}= maximum velocity in m/s, X=distance along the direction of flow from the tip of spur in m, Z=distance across the direction of flow from the tip of the spur in m

Table 4.2: Values of maximum velocities in m/s with their positions in m.

S.No.	Spur	A*	V_{app}	V_{max}	V_{max}/ V_{app}	X	Z
1	L1P1	0.111	0.25	0.363	1.452	0.8	0.45
2	L2P1	0.176	0.25	0.41	1.64	1.5	0.65
3	L3P1	0.25	0.25	0.46	1.84	1.9	0.75
4	L4P1	0.33	0.25	0.51	2.04	2.2	0.75
5	L1P2	0.086	0.25	0.34	1.36	0.05	0.2
6	L2P2	0.136	0.25	0.379	1.516	0.05	0.2
7	L3P2	0.19	0.25	0.412	1.648	0.05	0.2
8	L4P2	0.25	0.25	0.442	1.768	0.06	0.2

S.No.	Spur	A*	V_{app}	V_{max}	V_{max}/ V_{app}	X	Z
9	L1P3	0.063	0.25	0.326	1.304	0.06	0.2
10	L2P3	0.098	0.25	0.355	1.42	0.06	0.2
11	L3P3	0.136	0.25	0.383	1.532	0.06	0.2
12	L4P3	0.176	0.25	0.407	1.628	0.07	0.2
13	L1P4	0.041	0.25	0.303	1.212	0.1	0.25
14	L2P4	0.063	0.25	0.329	1.316	0.1	0.2
15	L3P4	0.086	0.25	0.342	1.368	0.1	0.25
16	L4P4	0.111	0.25	0.364	1.456	0.1	0.2
17	L1P5	0.02	0.25	0.277	1.108	0.1	0.3
18	L2P5	0.03	0.25	0.291	1.164	0.2	0.25
19	L3P5	0.041	0.25	0.302	1.208	0.25	0.25
20	L4P5	0.052	0.25	0.311	1.244	0.2	0.25
21	L1P1	0.111	0.3	0.436	1.453	0.8	0.45
22	L2P1	0.176	0.3	0.493	1.643	1.5	0.65
23	L3P1	0.25	0.3	0.554	1.847	2	0.75
24	L4P1	0.33	0.3	0.617	2.057	2.2	0.75
25	L1P2	0.086	0.3	0.404	1.347	0.05	0.2
26	L2P2	0.136	0.3	0.449	1.497	0.05	0.2
27	L3P2	0.19	0.3	0.486	1.620	0.05	0.2
28	L4P2	0.25	0.3	0.522	1.740	0.07	0.2
29	L1P3	0.063	0.3	0.386	1.287	0.06	0.2
30	L2P3	0.098	0.3	0.421	1.403	0.07	0.2
31	L3P3	0.136	0.3	0.449	1.497	0.1	0.2
32	L4P3	0.176	0.3	0.474	1.580	0.2	0.25
33	L1P4	0.041	0.3	0.359	1.197	0.15	0.25
34	L2P4	0.063	0.3	0.385	1.283	0.15	0.25
35	L3P4	0.086	0.3	0.400	1.333	0.15	0.25
36	L4P4	0.111	0.3	0.420	1.400	0.2	0.25
37	L1P5	0.02	0.3	0.329	1.097	0.2	0.3
38	L2P5	0.03	0.3	0.345	1.150	0.2	0.25
39	L3P5	0.041	0.3	0.357	1.190	0.25	0.25
40	L4P5	0.052	0.3	0.366	1.220	0.2	0.2

S.No.	Spur	A*	V_{app}	V_{max}	V_{max}/ V_{app}	X	Z
41	L1P1	0.111	0.4	0.582	1.455	0.8	0.45
42	L2P1	0.176	0.4	0.660	1.650	1.5	0.65
43	L3P1	0.25	0.4	0.740	1.850	2.2	0.75
44	L4P1	0.33	0.4	0.826	2.065	2.3	0.77
45	L1P2	0.086	0.4	0.532	1.330	0.06	0.2
46	L2P2	0.136	0.4	0.587	1.468	0.05	0.2
47	L3P2	0.19	0.4	0.636	1.590	0.06	0.2
48	L4P2	0.25	0.4	0.675	1.688	0.06	0.2
49	L1P3	0.063	0.4	0.504	1.260	0.1	0.2
50	L2P3	0.098	0.4	0.547	1.368	0.1	0.2
51	L3P3	0.136	0.4	0.582	1.455	0.1	0.2
52	L4P3	0.176	0.4	0.611	1.528	0.2	0.25
53	L1P4	0.041	0.4	0.469	1.173	0.15	0.25
54	L2P4	0.063	0.4	0.499	1.248	0.2	0.25
55	L3P4	0.086	0.4	0.523	1.308	0.2	0.25
56	L4P4	0.111	0.4	0.538	1.345	0.25	0.25
57	L1P5	0.02	0.4	0.438	1.095	0.3	0.3
58	L2P5	0.03	0.4	0.451	1.128	0.3	0.3
59	L3P5	0.041	0.4	0.462	1.155	0.4	0.25
60	L4P5	0.052	0.4	0.475	1.188	0.2	0.2

The following table contains the values of maximum shear stress τ_m and shear stress of undisturbed approach flow τ_0 in pascals at the bottom of the bed obtained numerically for all the cases near the tip of the spur. The maximum shear stress always came near the tip of the spur in all the cases.

Here τ_m= maximum shear stress near the tip of the spur, τ_0= undisturbed shear stress at the channel bed on the centreline before the effect of spur, τ_m/τ_0= shear stress amplification.

Table 4.3: Values of maximum shear stress in pascals.

S.No.	Spur	A*	V_{app}	τ_0	τ_m	τ_m/τ_0
1	L1P1	0.111	0.25	0.51	3.6	7.059
2	L2P1	0.176	0.25	0.51	3.7	7.255
3	L3P1	0.25	0.25	0.51	3.75	7.353
4	L4P1	0.33	0.25	0.51	3.9	7.647
5	L1P2	0.086	0.25	0.51	1.37	2.686
6	L2P2	0.136	0.25	0.51	1.44	2.824
7	L3P2	0.19	0.25	0.51	1.5	2.941
8	L4P2	0.25	0.25	0.51	1.47	2.882
9	L1P3	0.063	0.25	0.51	1.34	2.627
10	L2P3	0.098	0.25	0.51	1.34	2.627
11	L3P3	0.136	0.25	0.51	1.35	2.647
12	L4P3	0.176	0.25	0.51	1.4	2.745
13	L1P4	0.041	0.25	0.51	1.33	2.608
14	L2P4	0.063	0.25	0.51	1.22	2.392
15	L3P4	0.086	0.25	0.51	1.21	2.373
16	L4P4	0.111	0.25	0.51	1.23	2.412
17	L1P5	0.02	0.25	0.51	1.35	2.647
18	L2P5	0.03	0.25	0.51	1.13	2.216
19	L3P5	0.041	0.25	0.51	1	1.961
20	L4P5	0.052	0.25	0.51	1.03	2.020
21	L1P1	0.111	0.3	0.7	4.5	6.429
22	L2P1	0.176	0.3	0.7	4.55	6.500
23	L3P1	0.25	0.3	0.7	4.61	6.586
24	L4P1	0.33	0.3	0.7	4.76	6.800
25	L1P2	0.086	0.3	0.7	1.8	2.571
26	L2P2	0.136	0.3	0.7	1.86	2.657
27	L3P2	0.19	0.3	0.7	1.94	2.771
28	L4P2	0.25	0.3	0.7	1.89	2.700
29	L1P3	0.063	0.3	0.7	1.74	2.486
30	L2P3	0.098	0.3	0.7	1.66	2.371

S.No.	Spur	A*	V_{app}	τ_0	τ_m	τ_m/τ_0
31	L3P3	0.136	0.3	0.7	1.59	2.271
32	L4P3	0.176	0.3	0.7	1.72	2.457
33	L1P4	0.041	0.3	0.7	1.66	2.371
34	L2P4	0.063	0.3	0.7	1.56	2.229
35	L3P4	0.086	0.3	0.7	1.46	2.086
36	L4P4	0.111	0.3	0.7	1.49	2.129
37	L1P5	0.02	0.3	0.7	1.75	2.500
38	L2P5	0.03	0.3	0.7	1.43	2.043
39	L3P5	0.041	0.3	0.7	1.27	1.814
40	L4P5	0.052	0.3	0.7	1.3	1.857
41	L1P1	0.111	0.4	1.1	6	5.455
42	L2P1	0.176	0.4	1.1	6.09	5.536
43	L3P1	0.25	0.4	1.1	6.15	5.591
44	L4P1	0.33	0.4	1.1	6.21	5.645
45	L1P2	0.086	0.4	1.1	2.57	2.336
46	L2P2	0.136	0.4	1.1	2.7	2.455
47	L3P2	0.19	0.4	1.1	2.86	2.600
48	L4P2	0.25	0.4	1.1	2.78	2.527
49	L1P3	0.063	0.4	1.1	2.47	2.245
50	L2P3	0.098	0.4	1.1	2.5	2.273
51	L3P3	0.136	0.4	1.1	2.52	2.291
52	L4P3	0.176	0.4	1.1	2.54	2.309
53	L1P4	0.041	0.4	1.1	2.57	2.336
54	L2P4	0.063	0.4	1.1	2.22	2.018
55	L3P4	0.086	0.4	1.1	2.1	1.909
56	L4P4	0.111	0.4	1.1	1.94	1.764
57	L1P5	0.02	0.4	1.1	2.28	2.073
58	L2P5	0.03	0.4	1.1	1.91	1.736
59	L3P5	0.041	0.4	1.1	1.65	1.500
60	L4P5	0.052	0.4	1.1	1.82	1.655

The following table contains the values of Separation length obtained experimentally and numerically for all the cases.

Here L_{exp}=separation length obtained experimentally in m, L_{num}=separation length obtained numerically in m, l=length of spur in m.

Table 4.4: Values of separation length in m

S.No.	Spur	A*	V_{app}	L_{exp}	L_{exp}/l	L_{num}	L_{num}/l
1	L1P1	0.111	0.25	2.35	11.75	2.5	12.5
2	L2P1	0.176	0.25	3.60	12	3.78	12.6
3	L3P1	0.25	0.25	4.9	12.25	5.07	12.68
4	L4P1	0.33	0.25	6.2	12.4	6.38	12.75
5	L1P2	0.086	0.25	1.83	9.15	2	10
6	L2P2	0.136	0.25	2.8	9.33	2.94	9.8
7	L3P2	0.19	0.25	3.7	9.25	3.8	9.5
8	L4P2	0.25	0.25	4.7	9.4	4.8	9.6
9	L1P3	0.063	0.25	1.2	6	1.24	6.2
10	L2P3	0.098	0.25	-	-	1.82	6.08
11	L3P3	0.136	0.25	-	-	2.4	6
12	L4P3	0.176	0.25	-	-	2.95	5.91
13	L1P4	0.041	0.25	0.57	2.85	0.66	3.3
14	L2P4	0.063	0.25	0.95	3.15	0.98	3.26
15	L3P4	0.086	0.25	1	2.5	1.25	3.125
16	L4P4	0.111	0.25	-	-	1.48	2.96
17	L1P5	0.02	0.25	0.2	1	0.2	1
18	L2P5	0.03	0.25	0.48	1.59	0.5	1.66
19	L3P5	0.041	0.25	0.64	1.6	0.67	1.675
20	L4P5	0.052	0.25	-	-	1	2
21	L1P1	0.111	0.3	2.29	11.47	2.54	12.7
22	L2P1	0.176	0.3	3.51	11.70	3.84	12.8
23	L3P1	0.25	0.3	4.9	12.25	5.14	12.85
24	L4P1	0.33	0.3	6	12	6.45	12.9

S.No.	Spur	A*	V_{app}	L_{exp}	L_{exp}/l	L_{num}	L_{num}/l
25	L1P2	0.086	0.3	1.85	9.25	2	10
26	L2P2	0.136	0.3	2.70	9	2.94	9.8
27	L3P2	0.19	0.3	3.6	9	3.85	9.62
28	L4P2	0.25	0.3	4.8	9.6	4.75	9.5
29	L1P3	0.063	0.3	1.26	6.30	1.25	6.25
30	L2P3	0.098	0.3	1.67	5.58	1.75	5.83
31	L3P3	0.136	0.3	1.79	4.48	2.3	5.75
32	L4P3	0.176	0.3	-	-	2.85	5.7
33	L1P4	0.041	0.3	0.61	3.05	0.73	3.65
34	L2P4	0.063	0.3	0.97	3.23	1.03	3.45
35	L3P4	0.086	0.3	1.52	3.81	1.33	3.33
36	L4P4	0.111	0.3	-	-	1.62	3.25
37	L1P5	0.02	0.3	0.2	1	0.2	1
38	L2P5	0.03	0.3	0.46	1.53	0.5	1.66
39	L3P5	0.041	0.3	0.72	1.8	0.76	1.9
40	L4P5	0.052	0.3	-	-	0.98	1.96
41	L1P1	0.111	0.4	2.4	12	2.5	12.5
42	L2P1	0.176	0.4	3.6	12	3.78	12.6
43	L3P1	0.25	0.4	5	12.5	5.1	12.75
44	L4P1	0.33	0.4	6.25	12.5	6.4	12.8
45	L1P2	0.086	0.4	2.1	10.5	2	10
46	L2P2	0.136	0.4	2.9	9.67	3	10
47	L3P2	0.19	0.4	4.1	10.25	4	10
48	L4P2	0.25	0.4	5	10	5	10
49	L1P3	0.063	0.4	-	-	1.2	6
50	L2P3	0.098	0.4	-	-	1.8	6
51	L3P3	0.136	0.4	-	-	2.38	5.95
52	L4P3	0.176	0.4	-	-	2.92	5.85
53	L1P4	0.041	0.4	-	-	0.69	3.45
54	L2P4	0.063	0.4	-	-	1	3.33
55	L3P4	0.086	0.4	-	-	1.31	3.325
56	L4P4	0.111	0.4	-	-	1.58	3.16

S.No.	Spur	A*	V_{app}	L_{exp}	L_{exp}/l	L_{num}	L_{num}/l
57	L1P5	0.02	0.4	-	-	0.2	1
58	L2P5	0.03	0.4	-	-	0.51	1.7
59	L3P5	0.041	0.4	-	-	0.72	1.8
60	L4P5	0.052	0.4	-	-	1	2

4.2 Software plots

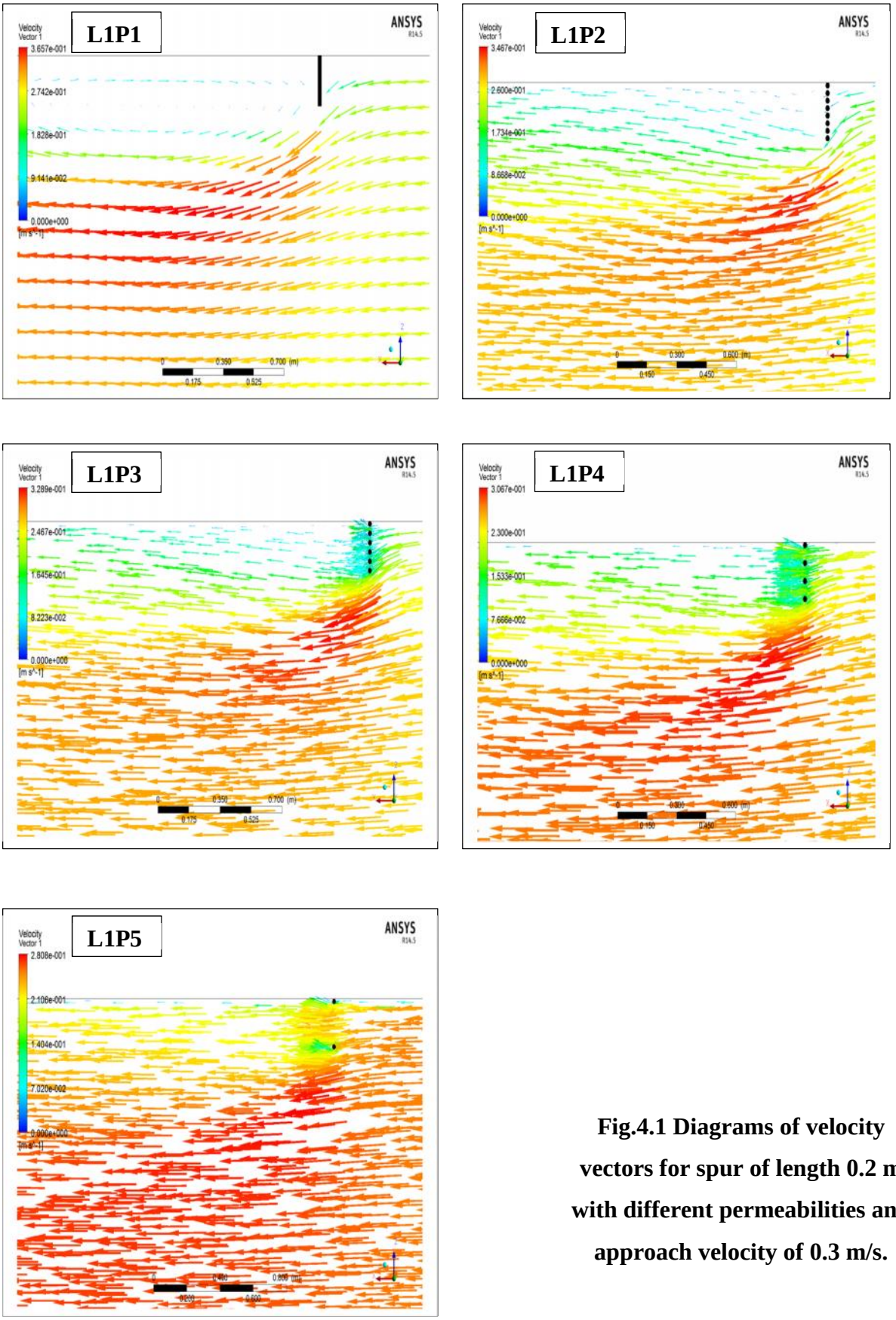

Fig.4.1 Diagrams of velocity vectors for spur of length 0.2 m with different permeabilities and approach velocity of 0.3 m/s.

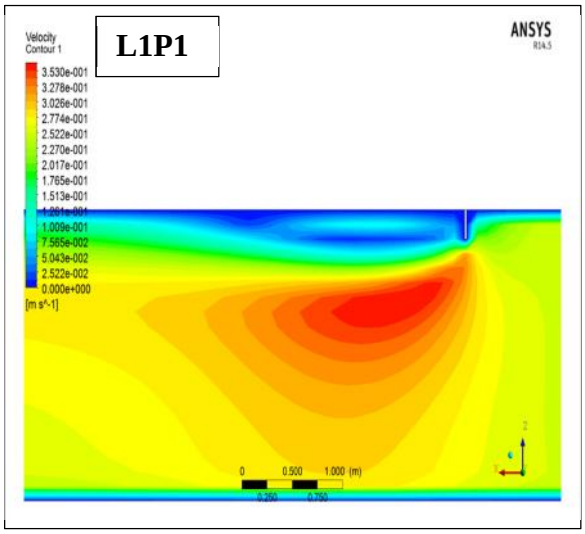

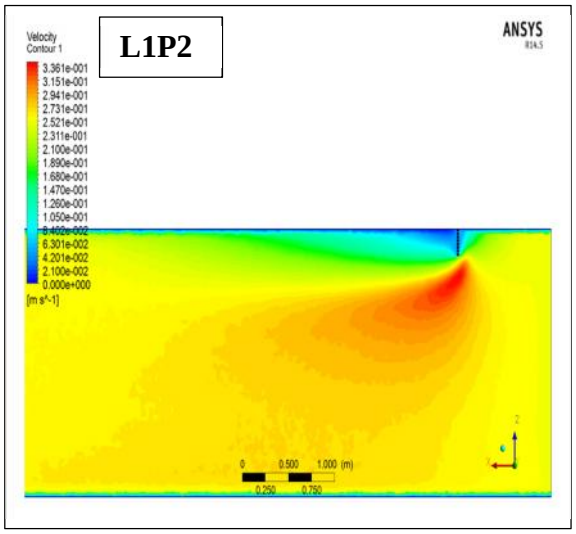

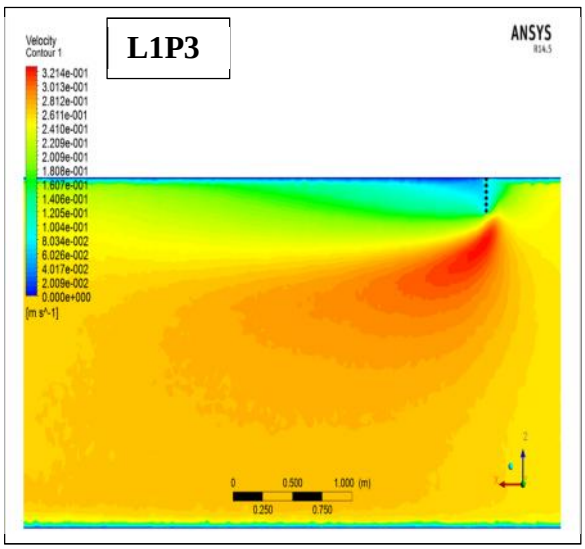

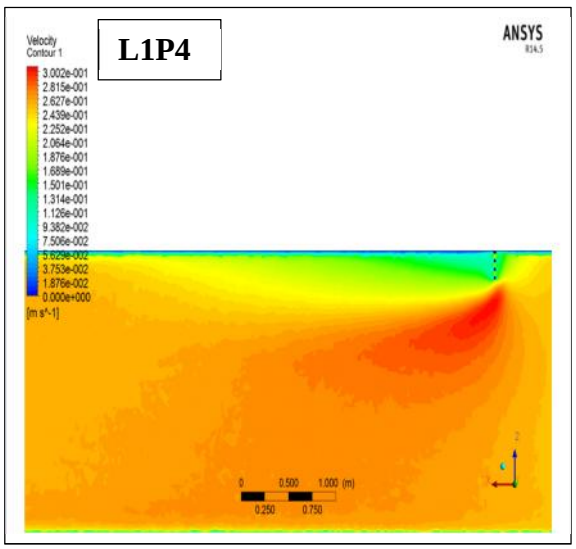

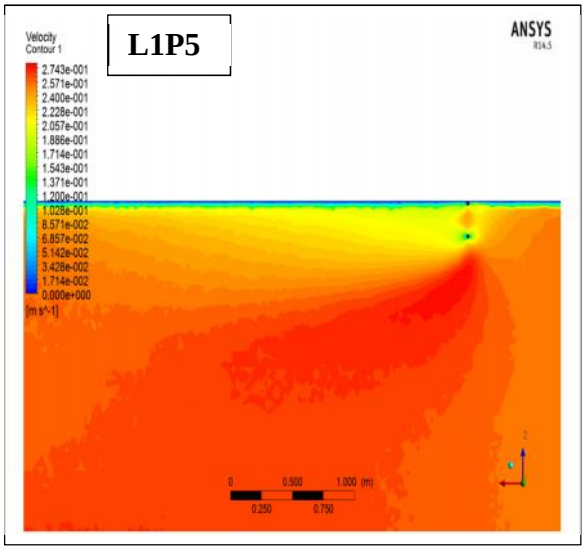

Fig.4.2 Diagrams of velocity contours for spur of length 0.2 m with different permeabilities and approach velocity of 0.3 m/s.

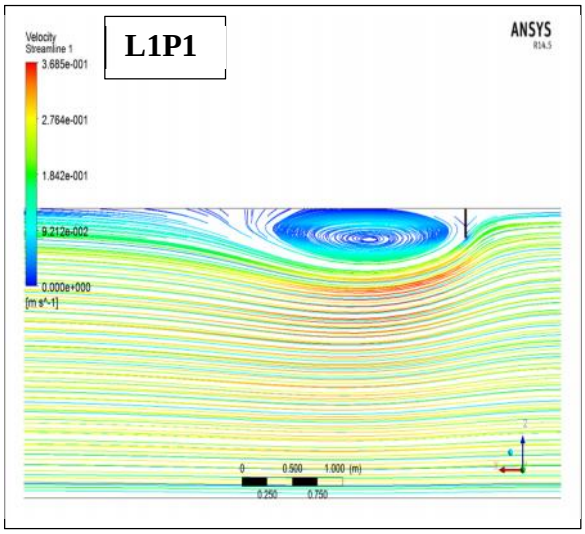

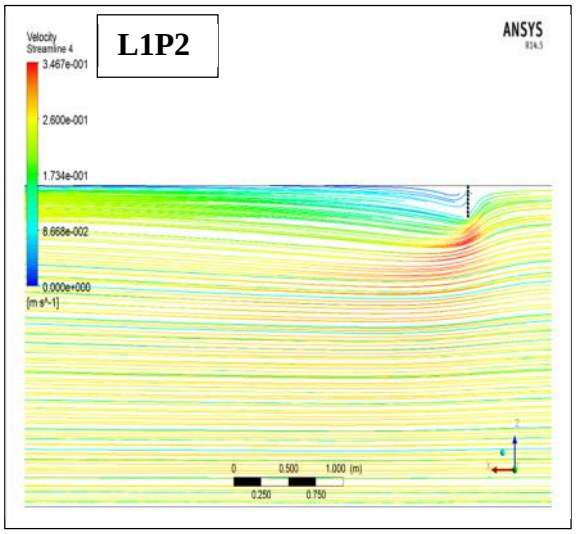

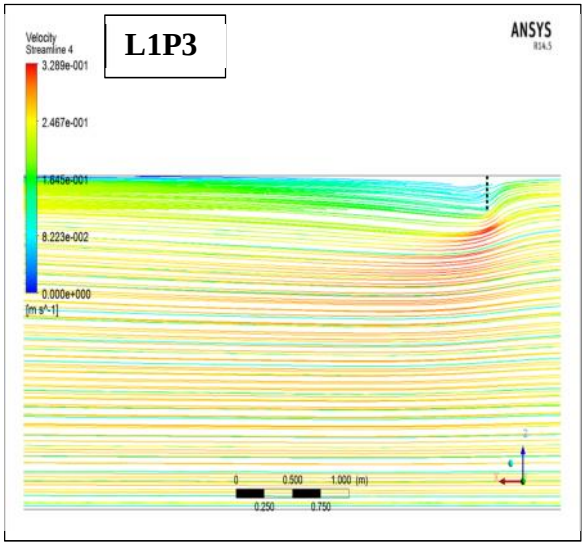

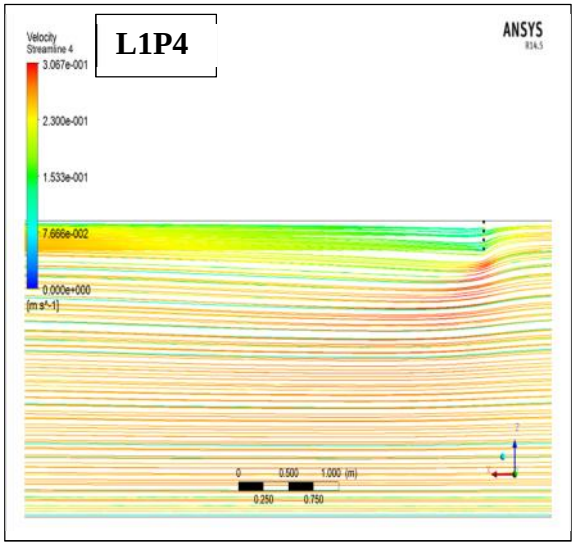

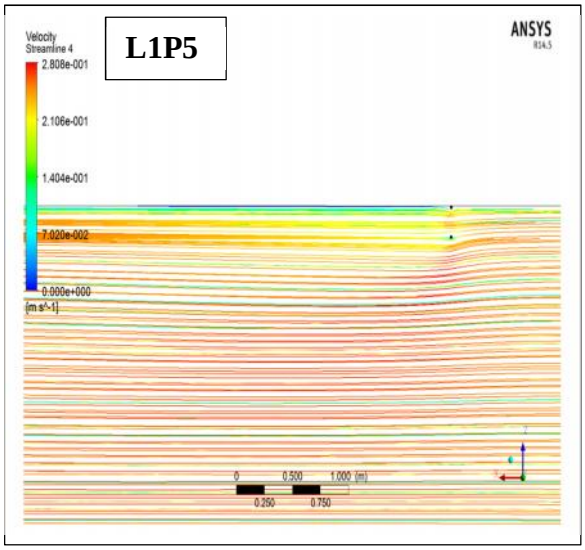

Fig.4.3 Diagrams of streamlines for spur of length 0.2 m with different permeabilities and approach velocity of 0.3 m/s.

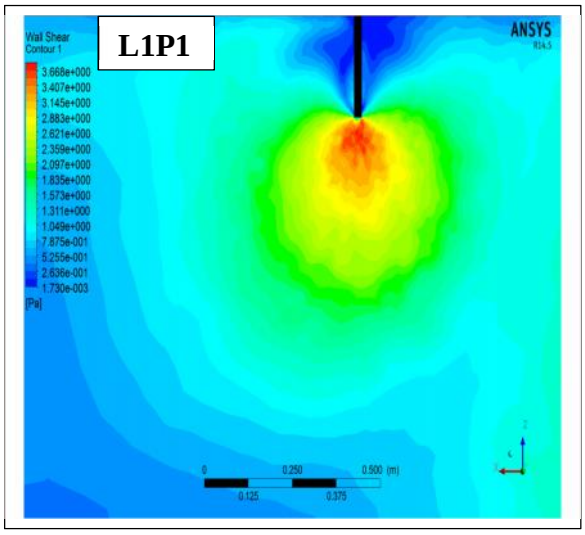

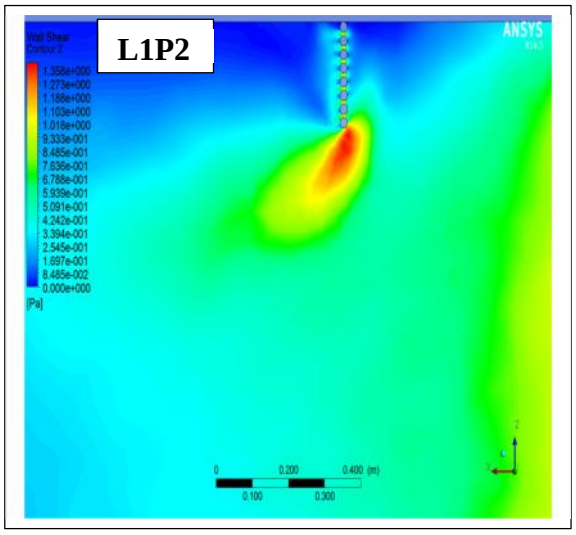

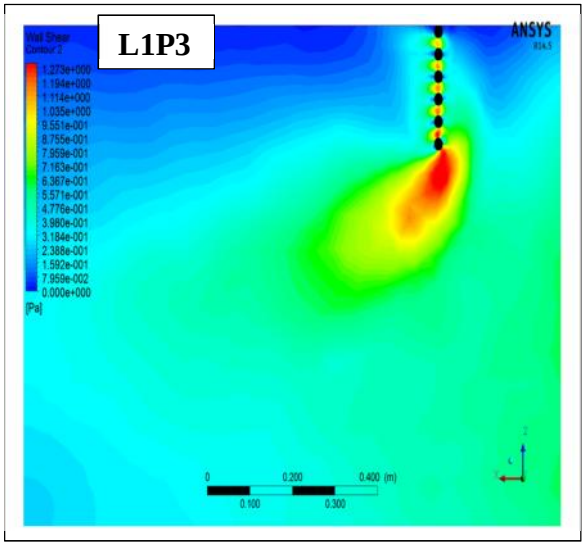

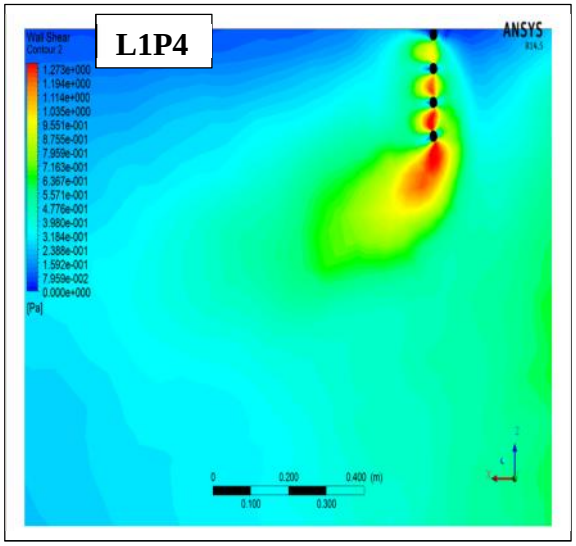

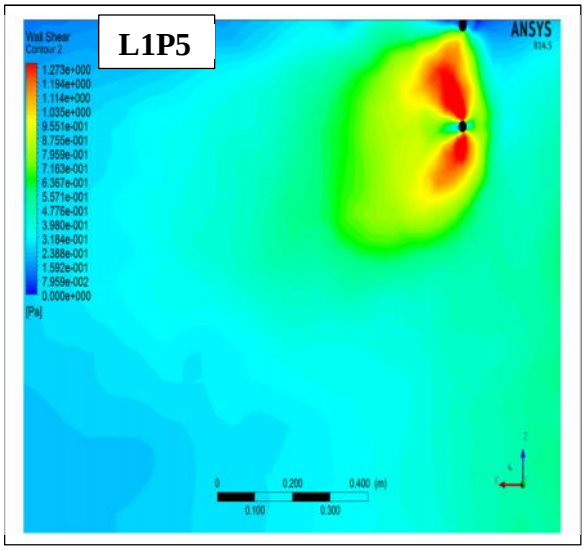

Fig.4.4 Diagrams of bed shear stress for spur of length 0.2 m with different permeabilities and approach velocity of 0.3 m/s.

CHAPTER 5-RESULTS AND DISCUSSIONS

5.1 Results based on Tip velocity

Here the results based on tip velocity are presented. The flow at the tip of spur was steeply changed to the centre of the channel and the intensive vortex formed at the tip leads to local scour. So we focus our attention here on the variation of tip velocity with change in spur length and permeability. The tip velocity was measured at the middle layer (60% of the water depth).

Fig.5.1, 5.2, 5.3 shows the graph between tip velocity and spur length for different permeabilities. The tip velocity increased from 1.25 times to 1.7 times the approach velocity as the length of spur is increased. The tip velocity increased with spur length in every case of numerical results. But in case of experimental results, the tip velocity decreased as we increase the spur length for 60% and 80% permeability. The relative error of the tip velocity between experimental and numerical results is always less than 10%. The error becomes less as the approach velocity is increased. In Fig.5.3, tip velocities follow same pattern but they differ in magnitude. So as the velocity increases, the numerical values converge towards experimental values

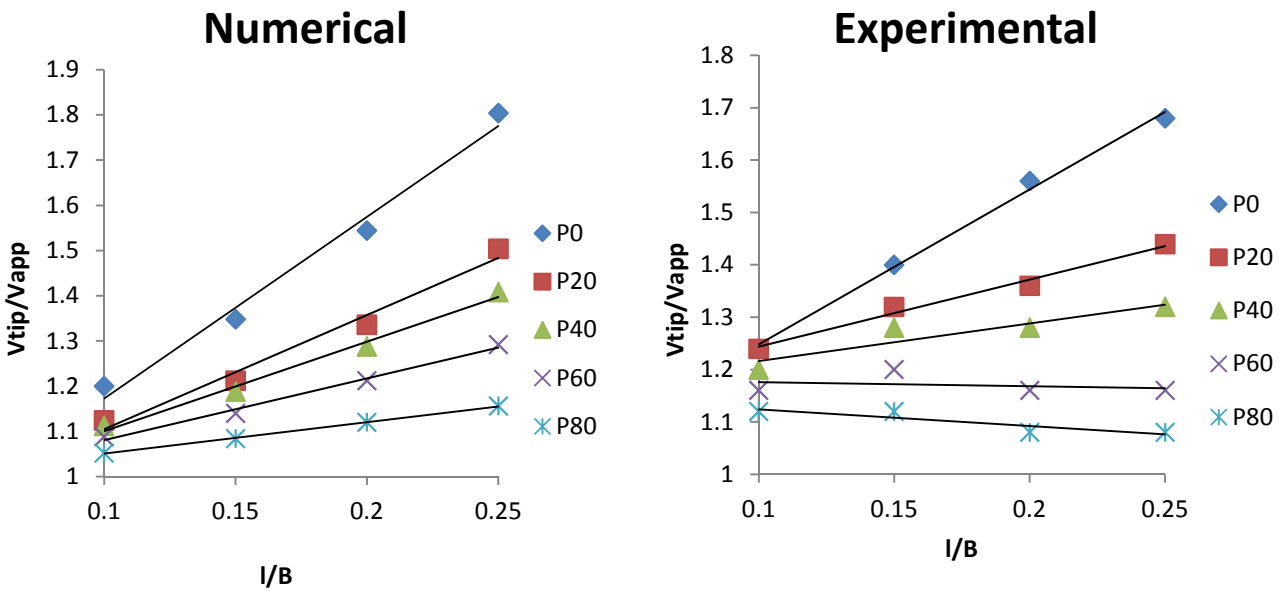

Fig.5.1 Tip velocity and spur length variation with permeability for approach velocity 0.25m/s

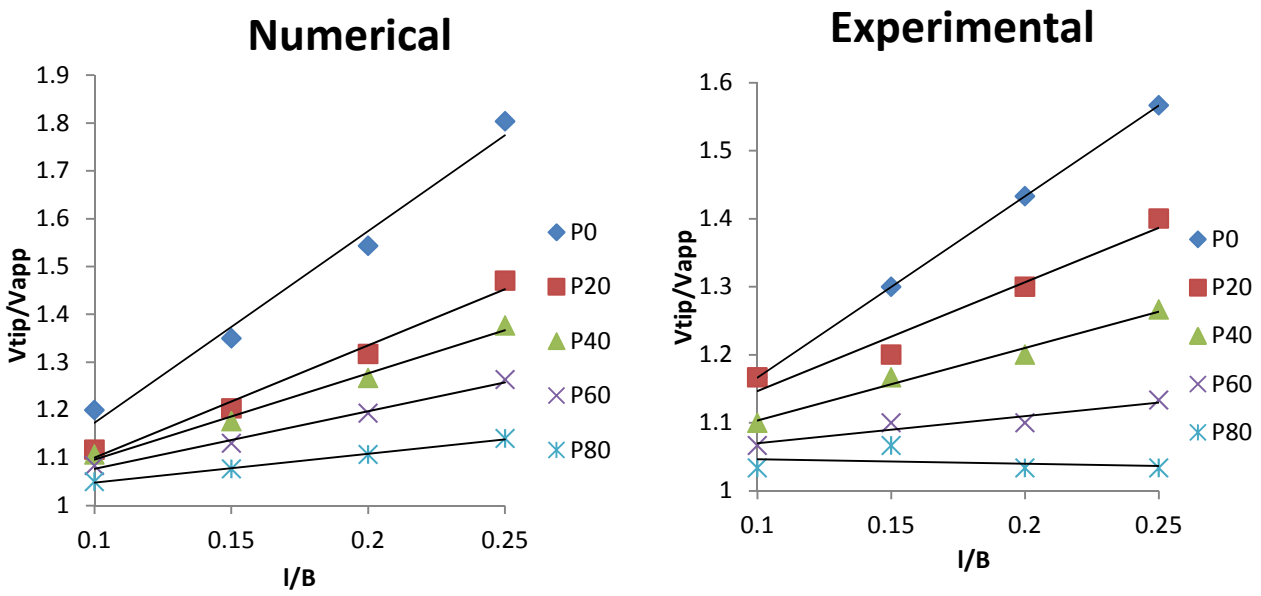

Fig.5.2 Tip velocity and spur length variation with permeability for approach velocity 0.30m/s

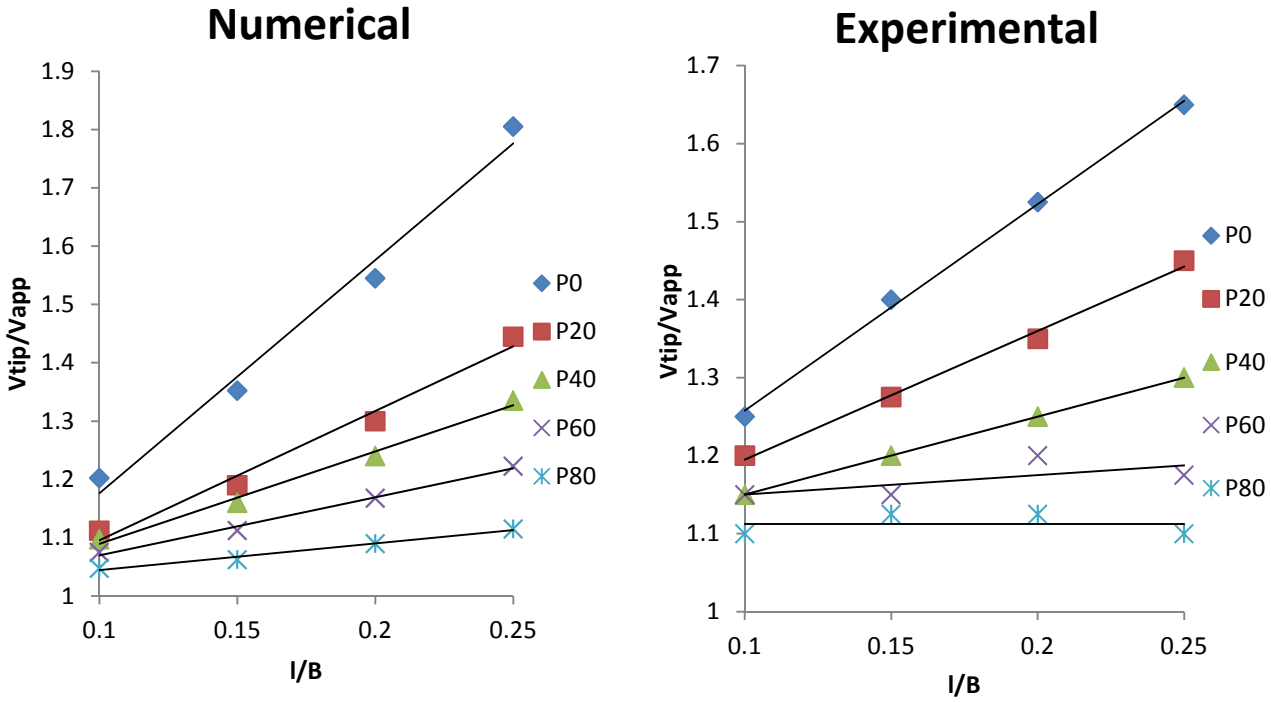

Fig.5.3 Tip velocity and spur length variation with permeability for approach velocity 0.40m/s

Fig.5.4, 5.5, 5.6 shows the graph between tip velocity and permeability with different spur lengths. The tip velocity gets reduced in every case as the permeability is increased due to more flow between the spurs. The length of spur has considerable effect in impermeable spur in increasing the tip velocity. But as the permeability is introduced in the spurs, the tip velocity begins to converge. As it can be seen from the graphs that tip velocity for 80% permeability is almost same in all the cases of spur length. Hence it can be said that the spur of 80% permeability behaves like a cylindrical pier in the channel. So the impermeable spur has more tip velocity than permeable spur and therefore is more susceptible to local scour at the tip. Therefore it can said that the numerical results present satisfying agreement with the experimental results.

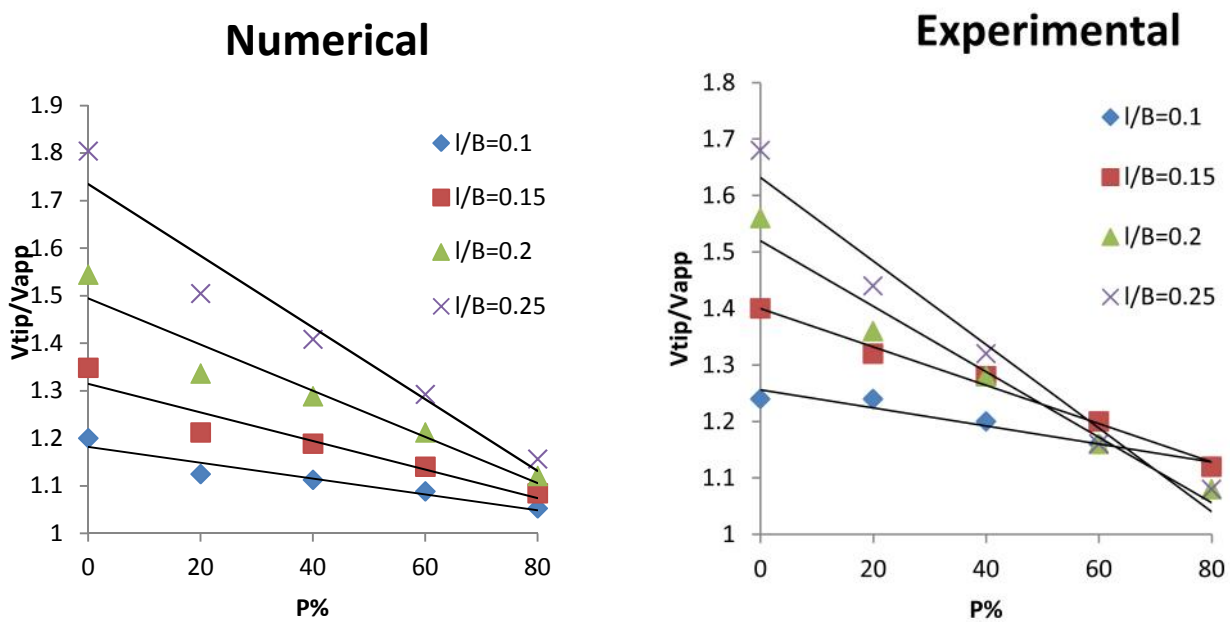

Fig.5.4 Tip velocity and permeability variation with spur length for approach velocity 0.25m/s

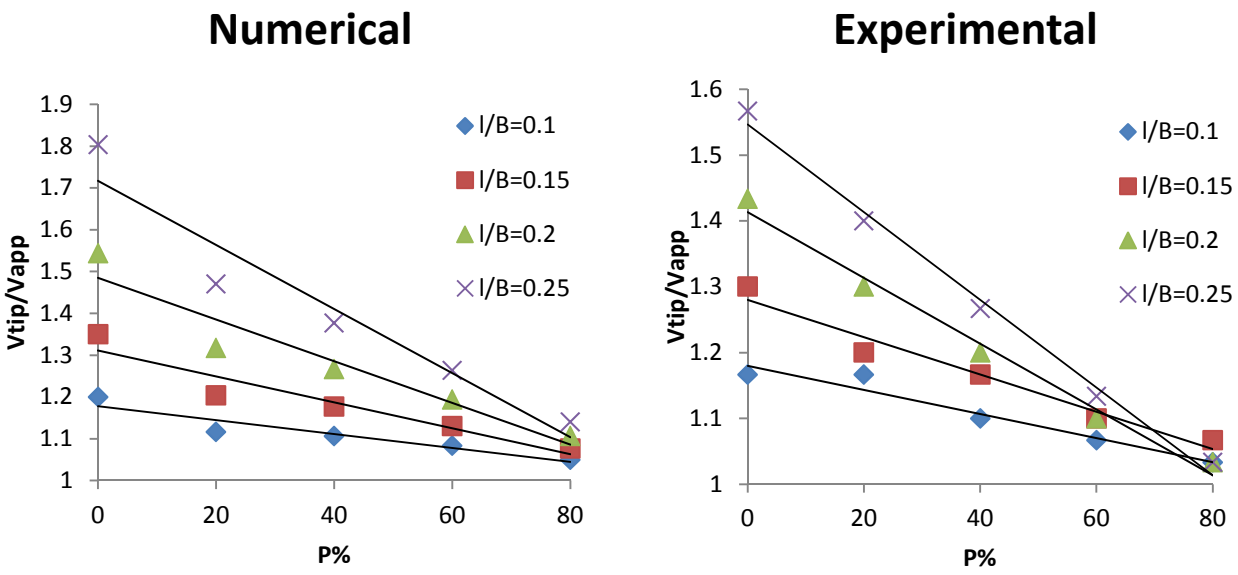

Fig.5.5 Tip velocity and permeability variation with spur length for approach velocity 0.30m/s

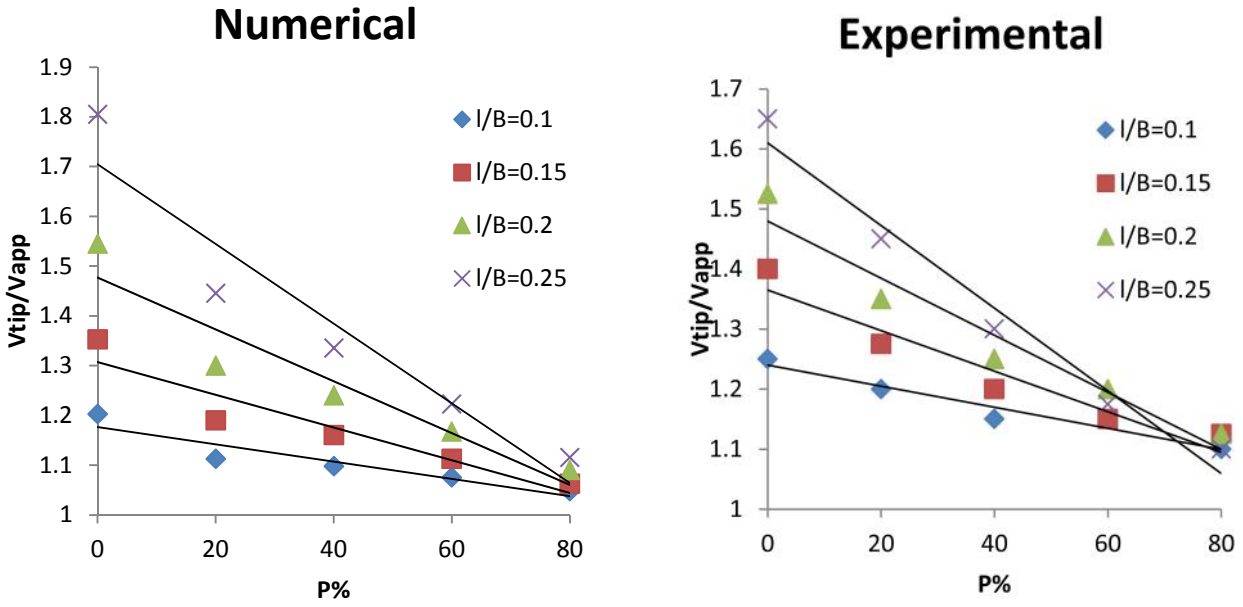

Fig.5.6 Tip velocity and permeability variation with spur length for approach velocity 0.40m/s

Fig.5.7 shows the numerical data being compared with the design guidelines given by Wallingford. The numerical data is well within the range of the lines of Wallingford. W1 refers to the $S_L/l=6$ and W2 refers to the $S_L/l=10$ (S_L/l is ratio of separation length and spur length). Fig.5.8 shows the same comparison but with the experimental data. The experimental results are also within the range and results are reasonable. The numerical results have less scatter as compared to the experimental results.

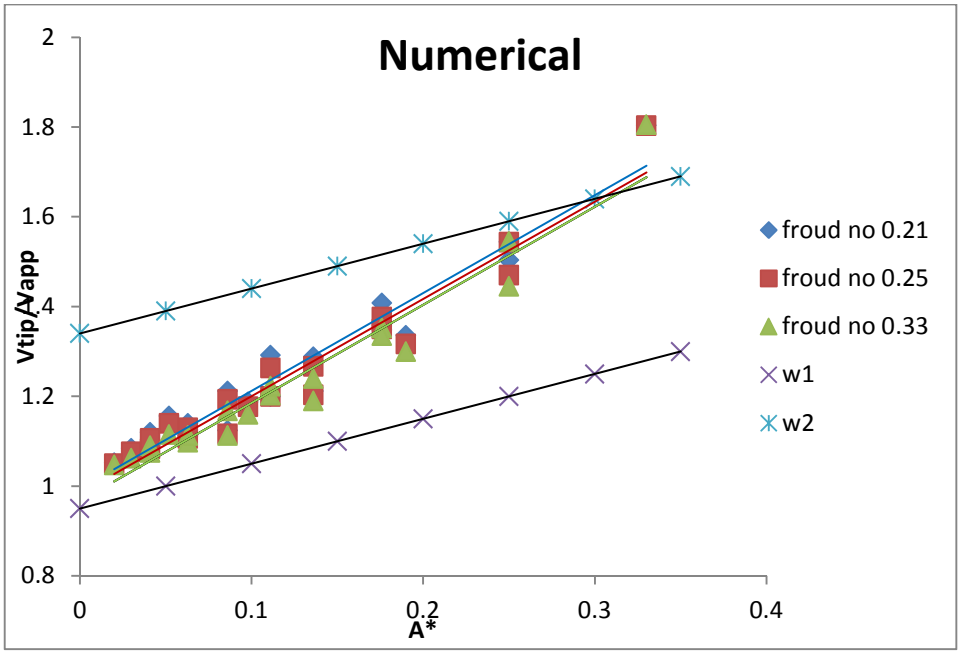

Fig.5.7 Comparing Wallingford to numerical data

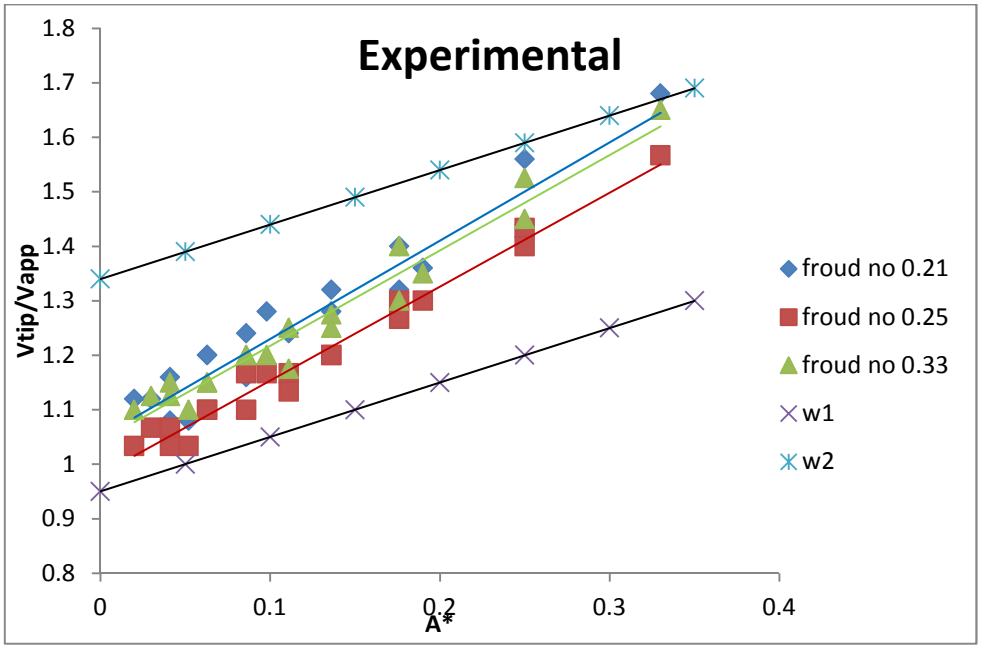

Fig.5.8 Comparing Wallingford to experimental data

Fig.5.9 shows the plot of experimental versus numerical tip velocities. The correlation comes put to be 0.92 which is considerably good.

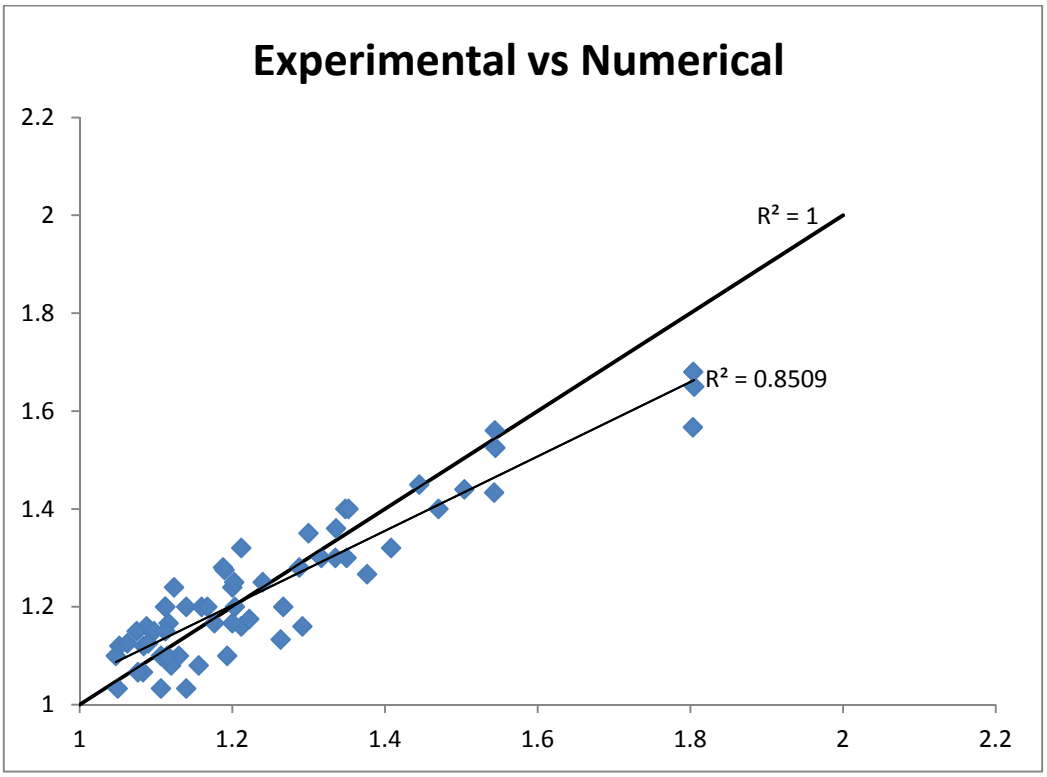

Fig.5.9 Comparison between experimental and numerical data for tip velocities

Fig.5.10 shows the empirical equation developed by Yeo et al. [27]. By using the experimental data, the empirical equation comes out to be

$$\frac{V_{tip}}{V_{app}} = 1.76 \times A^* + 1.015 \qquad \text{.....Eq.5.1}$$

Where A* is area ratio and is equal to

$$A^* = \frac{A_g}{A_c - A_g} \qquad \text{for } 0.02<A^*<0.35$$

Here A_g is the lateral projecting area of spur on the channel cross section

And A_c is the cross sectional area of flow in channel.

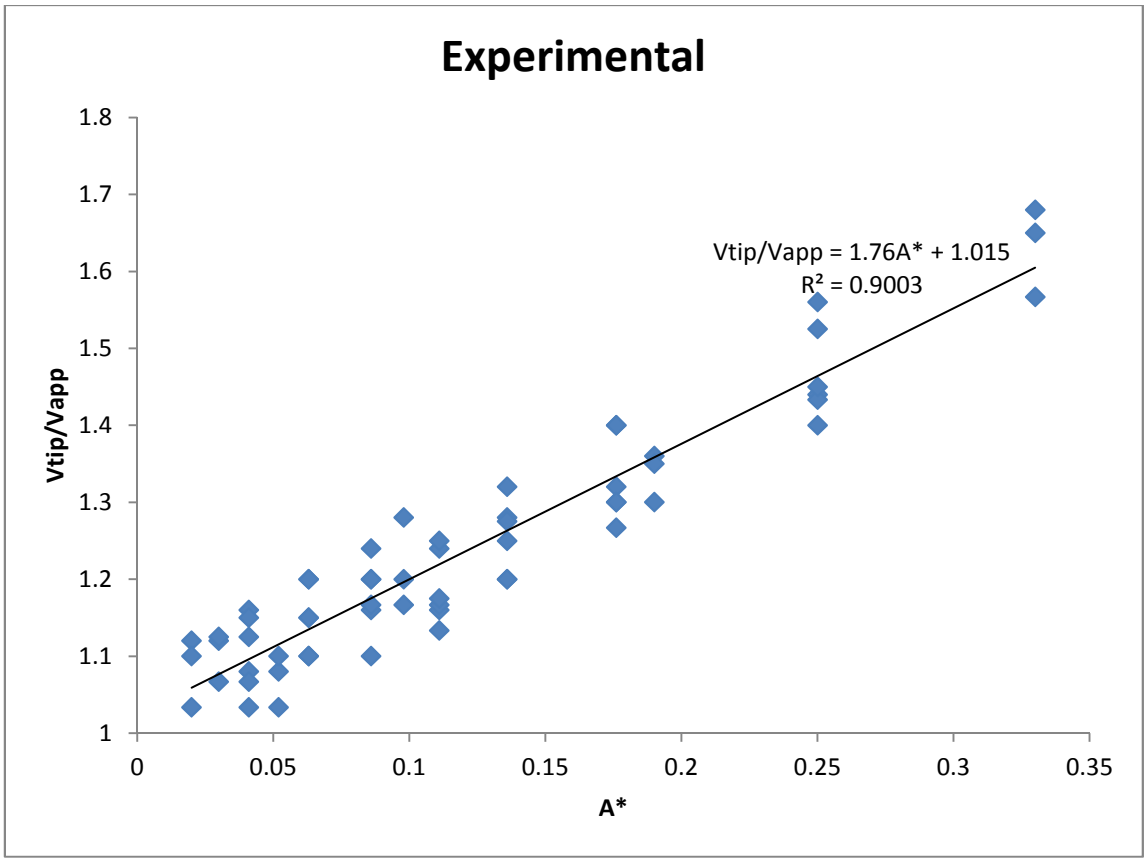

Fig.5.10 Empirical equation for tip velocity for experimental data

The above equation was modified by introducing permeability as a variable in the system. Then multiple regression analysis was performed with Vtip/Vapp taken as dependent variable and A*, P taken as independent variable. The correlation coefficient R comes out to be 0.97 which shows good relationship among the variables. The value of adjusted R square comes out to be 0.95 which means 95% of the values fit the equation. The value of significance F is less than 0.05 which means the equation is ok. Also all the P-values are less than 0.05 which means the independent variables used are good to be used.

Table 5.1 Multiple regression analysis for tip velocity

SUMMARY OUTPUT

Regression Statistics	
Multiple R	0.978566
R Square	0.957591
Adjusted R Square	0.956102
Standard Error	0.038886
Observations	60

ANOVA

	df	*SS*	*MS*	*F*	*Significance F*
Regression	2	1.946156	0.973078	643.5195	7.63E-40
Residual	57	0.086191	0.001512		
Total	59	2.032347			

	Coefficients	*Standard Error*	*t Stat*	*P-value*	*Lower 95%*	*Upper 95%*
Intercept	0.881312	0.022618	38.96456	8.87E-43	0.83602	0.926605
P	0.136852	0.028417	4.815797	1.12E-05	0.079948	0.193757
A*	2.54833	0.098144	25.96517	2.86E-33	2.3518	2.744861

The modified equation comes out to be:

$$\frac{V_{tip}}{V_{app}} = 0.881 + 0.136 \times P + 2.548 \times A^{*} \qquad \text{.....Eq.5.2}$$

With the help of Eq.5.2 the predicted values of Vtip/Vapp were found out and compared with the experimental values in Fig.5.11. The R value comes out to be 0.93 which is good.

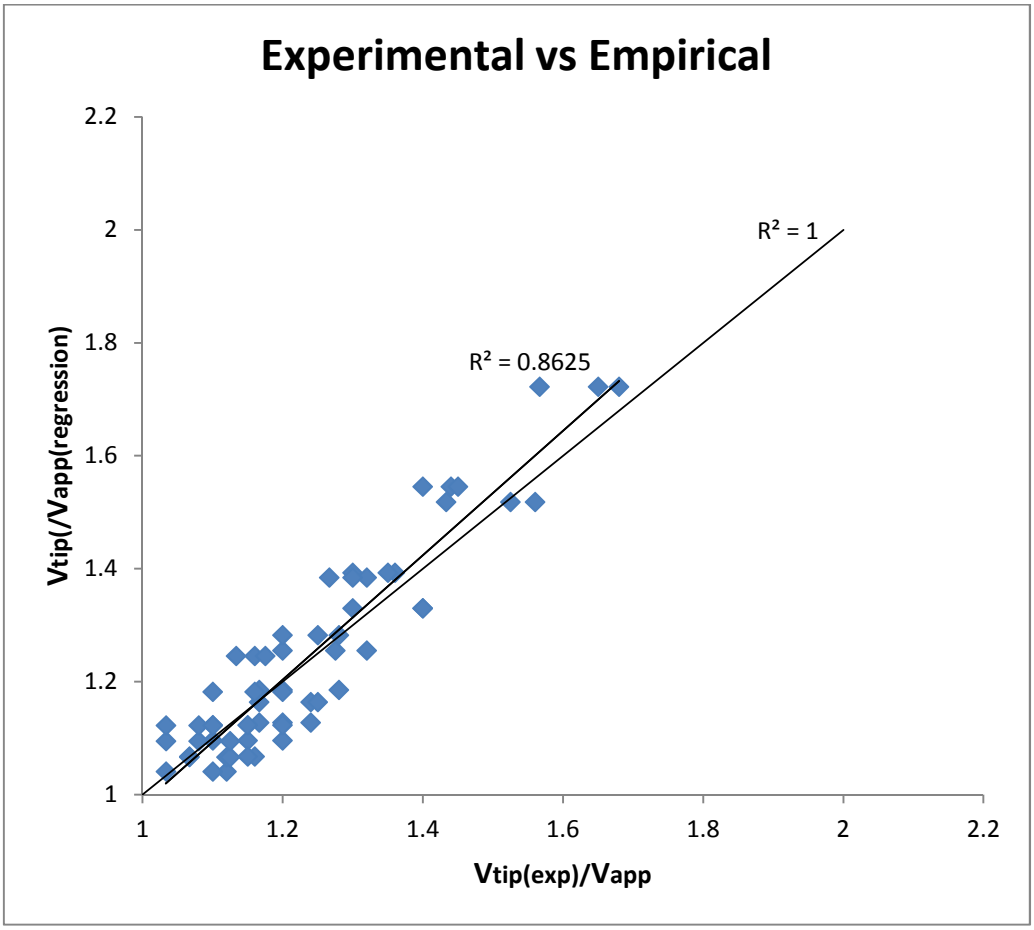

Fig.5.11 Plot of predicted values (Regression Eq.5.2) vs experimental values

5.2 Results based on Separation length

The separation length is the length of recirculation zone or when the separated flow returns to the main flow. It can be useful in deciding the installation interval when series of spurs are placed in a channel.

Fig.5.12, 5.13, 5.14 shows the variation of separation length and spur length with different permeabilities for different approach velocities. The separation length was maximum for impermeable spur and it comes out to be 12.5 times spur length on the average. The separation length is 10 times the spur length for 20% permeability,5.7 times the spur length for 40% permeability, 3 times the spur length for 60%

permeability and about 1.8 times the spur length for 80% permeability. Increasing the spur length increases the separation length. The numerical data is also in good agreement with the experimental data. The relative error of separation length for numerical and experimental results is less than 5% in all cases.The recirculation zone was formed only in impermeable spur. There was no such pattern in permeable spurs(Fig.4.3).

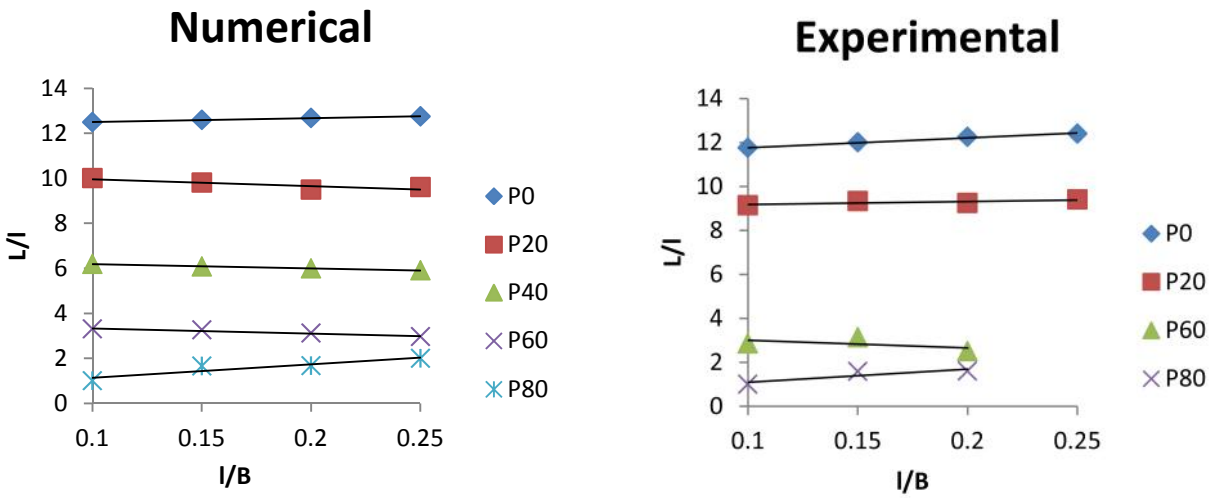

Fig.5.12 Separation length and spur length variation with permeability for approach velocity 0.25m/s

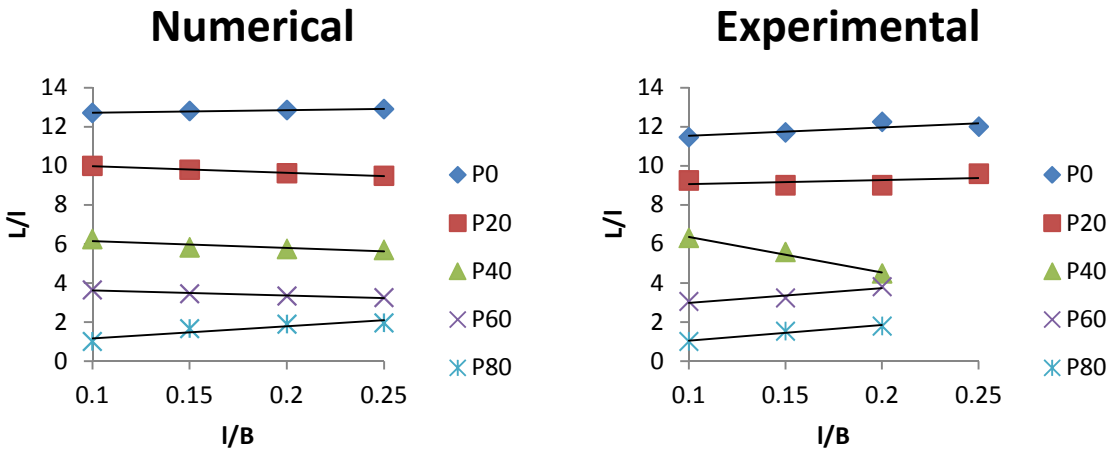

Fig.5.13 Separation length and spur length variation with permeability for approach velocity 0.30m/s

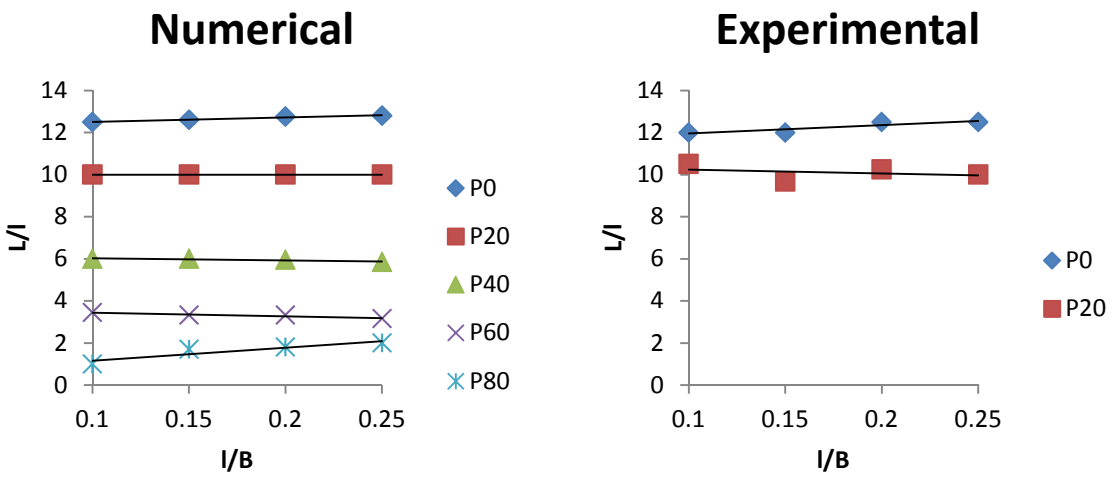

Fig.5.14 Separation length and spur length variation with permeability for approach velocity 0.40m/s

Fig.5.15, 5.16, 5.17 shows the variation of separation length and permeability with different spur lengths for different approach velocities. There were some missing values of separation length which has been found numerically.

Based on the results of separation length and tip velocity, it can be said that ANSYS Fluent can be used for flow analysis near a spur. So here ANSYS Fluent has been used to determine maximum velocity and its location with respect to the tip of the spur. Also it has been used to determine the maximum bed shear stress near the spur. These data were not calculated in experiments and has been calculated here to further understand the effect of permeability.

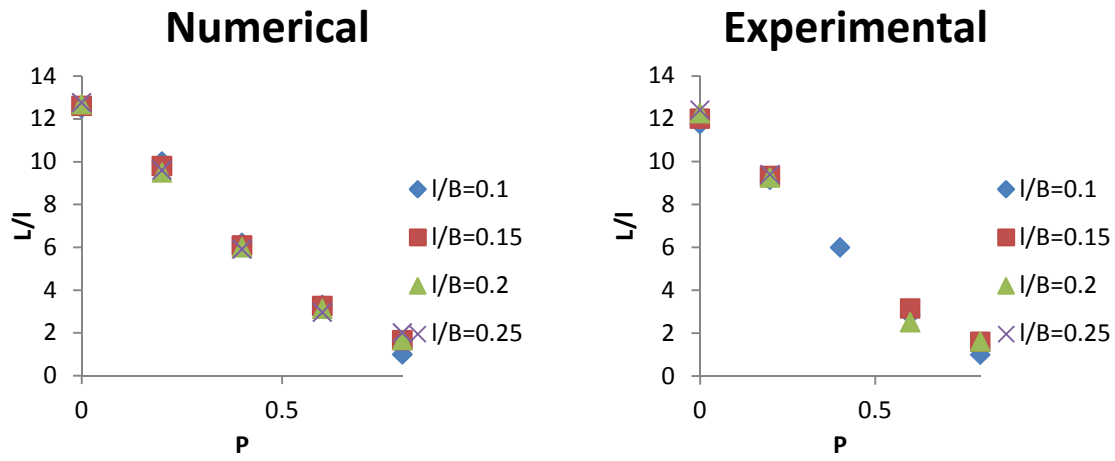

Fig.5.15 Separation length and permeability variation with spur length for approach velocity 0.25m/s

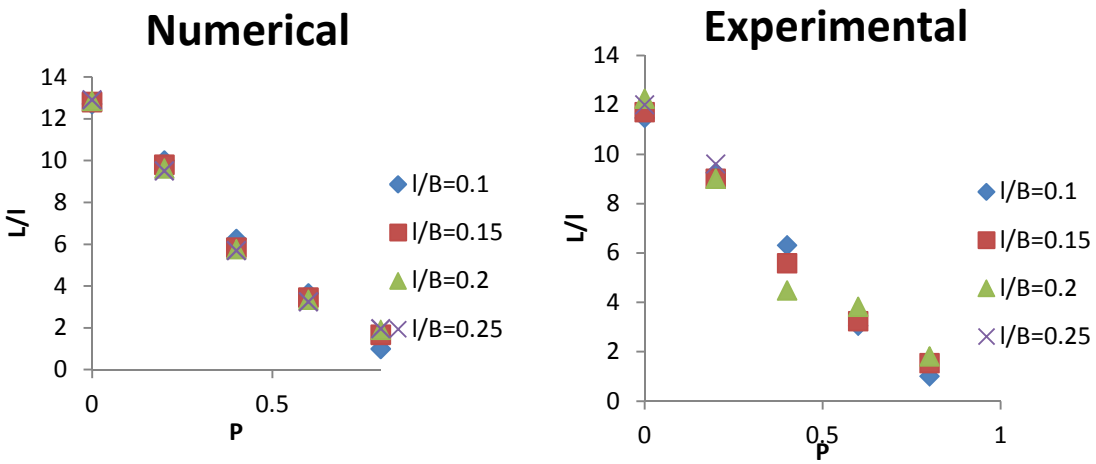

Fig.5.16 Separation length and permeability variation with spur length for approach velocity 0.30m/s

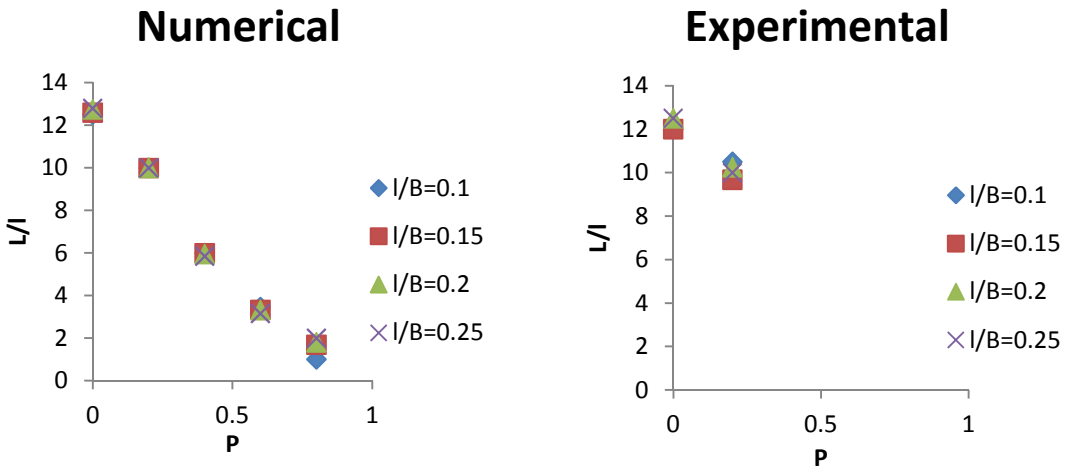

Fig.5.17 Separation length and permeability variation with spur length for approach velocity 0.40m/s

5.3 Results based on Maximum velocity

The point of maximum velocity can be some idea where the maximum scour depth is formed. For impermeable spur, the maximum velocity point was at a distance of five times the spur length in the direction of flow and two times the spur length across the flow from the tip of the spur, which means the maximum scour depth was formed away from the tip of the spur. For the permeable spurs, the maximum velocity point was two times the spur length in both along the flow and across the flow directions, which means the maximum scour depth was somewhere near the tip of the spur.

A multiple regression analysis was carried out with Maximum velocity as dependent variable and A*, P as the dependent variables. The correlation coefficient R comes out to be 0.99 which shows very good relationship among the variables. The value of adjusted R square comes out to be 0.98 which means 98% of the values fit the equation. The value of significance F is less than 0.05 which means the equation is ok. Also all the P-values are less than 0.05 which means the independent variables used are good to be used.

Table 5.2 Multiple regression analysis of maximum velocity

SUMMARY OUTPUT

Regression Statistics	
Multiple R	0.991492
R Square	0.983057
Adjusted R Square	0.982463
Standard Error	0.032521
Observations	60

ANOVA

	df	*SS*	*MS*	*F*	*Significance F*
Regression	2	3.49786	1.74893	1653.625	3.36E-51
Residual	57	0.060285	0.001058		
Total	59	3.558145			

	Coefficients	*Standard*	*t Stat*	*P-value*	*Lower 95%*	*Upper*

		Error				*95%*
Intercept	1.16522	0.018916	61.59891	7.54E-54	1.12734	1.203099
A*	2.625812	0.08208	31.99075	4.16E-38	2.461449	2.790175
P	-0.11562	0.023766	-4.86491	9.41E-06	-0.16321	-0.06803

The empirical equation comes out to be:

$$\frac{V_{max}}{V_{app}} = 1.165 + 2.625 \times A^* - 0.115 \times P \qquad \text{.....Eq.5.3}$$

5.4 Results based on Maximum bed shear stress

The analysis of shear stress field on the bed of the channel presents interests for studying the sediment transport around a spur. Downstream from a spur dike in the recirculation zone, bed shear stresses decrease and deposition occurs in this zone. Near the tip of the spur, velocity and bed shear stress increase and bed erosion occurs.

Fig.5.18, 5.19, 5.20 shows the variation of maximum bed shear stress and spur length with different permeabilities. Increasing the spur length has negligible effect on the bed shear stress. The bed shear stress is more for impermeable spurs.

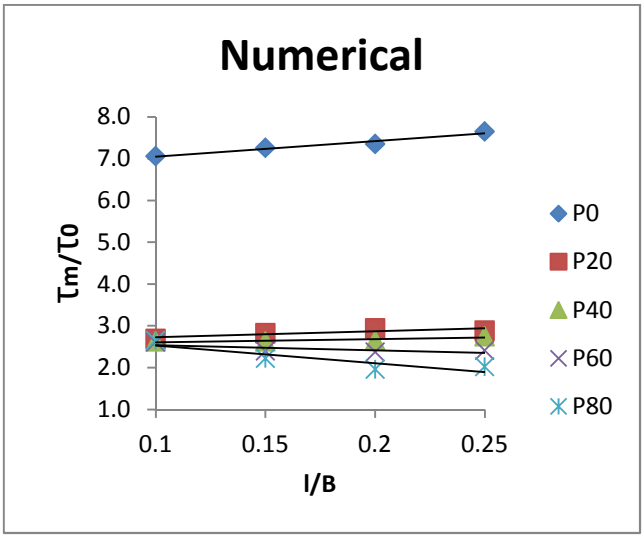

Fig.5.18 Maximum bed shear stress and spur length variation with permeability for approach velocity 0.25m/s

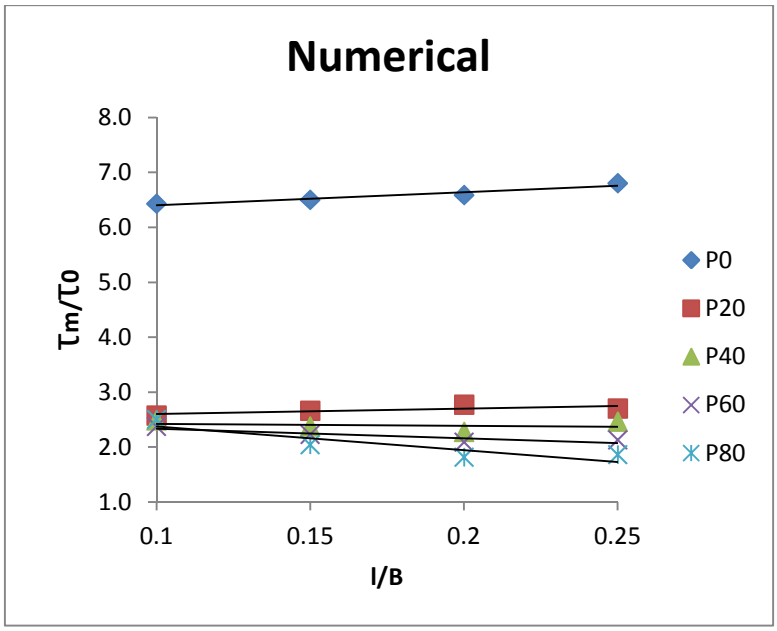

Fig.5.19 Maximum bed shear stress and spur length variation with permeability for approach velocity 0.30m/s

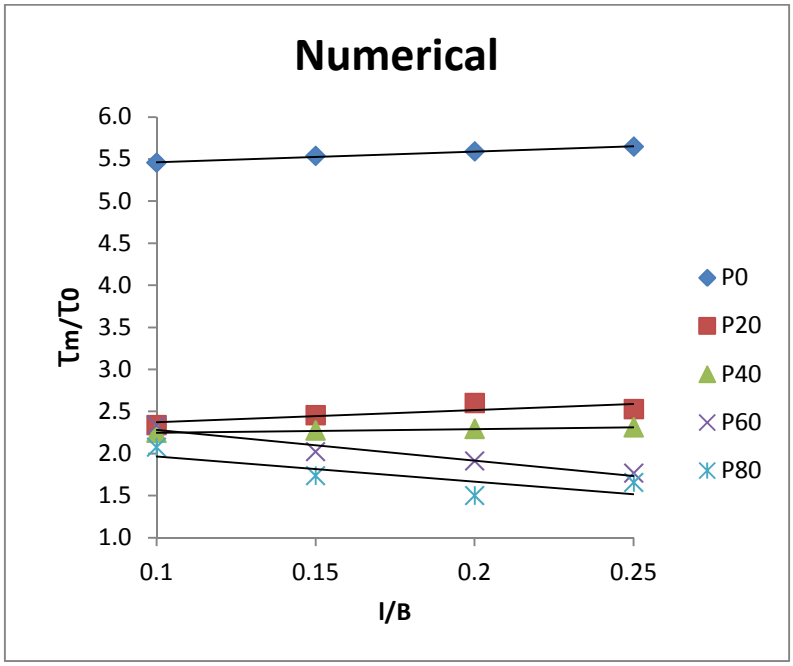

Fig.5.20 Maximum bed shear stress and spur length variation with permeability for approach velocity 0.40m/s

Fig.5.21, 5.21, 5.23 shows the variation of bed shear stress and permeability with different spur lengths for different approach velocities. For all permeable spurs

maximum bed shear stress is in the same range. Upto 20% permeability a remarkable change is observed in corresponding values. The permeability effect becomes lesser and lesser important with change in P with further change in the values.

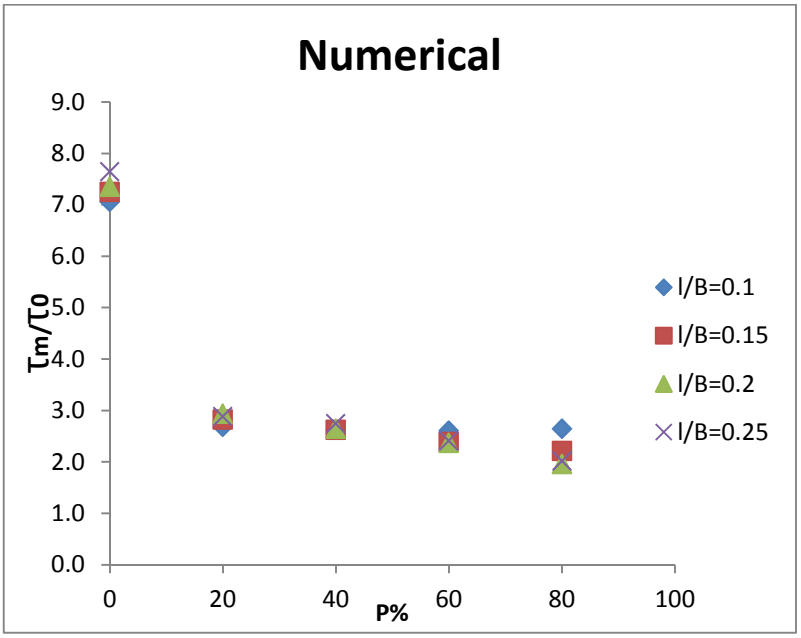

Fig.5.21 Maximum bed shear stress and permeability variation with spur length for approach velocity 0.25m/s

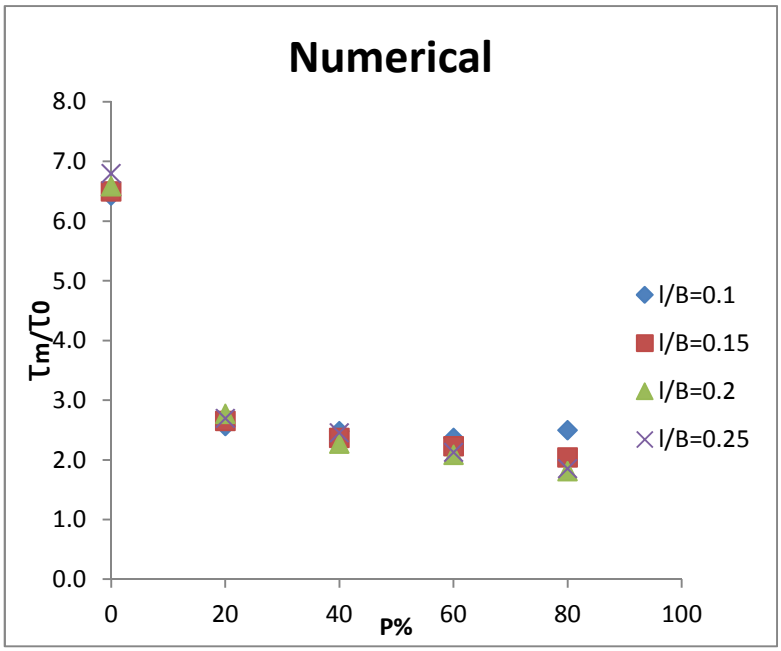

Fig.5.22 Maximum bed shear stress and permeability variation with spur length for approach velocity 0.30m/s

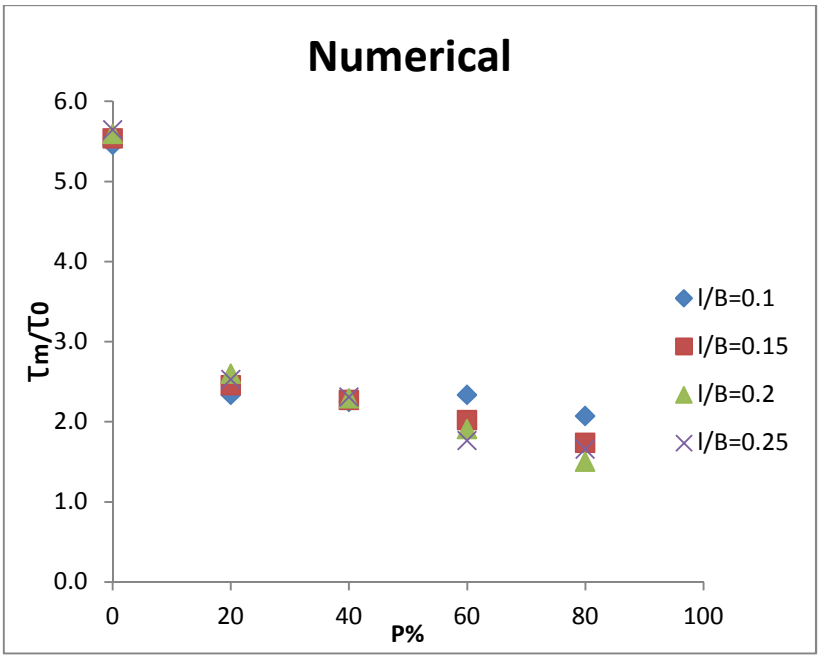

Fig.5.23 Maximum bed shear stress and permeability variation with spur length for approach velocity 0.40m/s

A multiple regression analysis was carried out with Maximum bed shear stress as dependent variable and A*, P, Vtip/Vapp as the dependent variables. Here Vtip/Vapp can be calculated from the previous relationship given in 5.1.The correlation coefficient R comes out to be 0.91 which shows satisfying relationship among the variables. The value of adjusted R square comes out to be 0.82 which means 82% of the values fit the equation. The value of significance F is less than 0.05 which means the equation is ok. Also all the P-values are less than 0.05 which means the independent variables used are good to be used.

Table 5.3 Multiple regression analysis of maximum bed shear stress

SUMMARY OUTPUT

Regression Statistics	
Multiple R	0.912657
R Square	0.832942
Adjusted R Square	0.823993
Standard Error	0.729915
Observations	60

ANOVA

	df	*SS*	*MS*	*F*	*Significance F*
Regression	3	148.7581	49.58605	93.07106	9.64E-22
Residual	56	29.83547	0.532776		
Total	59	178.5936			

	Coefficients	*Standard Error*	*t Stat*	*P-value*	*Lower 95%*	*Upper 95%*
Intercept	-14.7036	2.230281	-6.59269	1.63E-08	-19.1714	-10.2358
P	-7.31296	0.632791	-11.5567	1.87E-16	-8.58059	-6.04532
A*	-54.2274	6.598025	-8.21873	3.38E-11	-67.4448	-41.0099
Vtip/Vapp	21.98358	2.485352	8.845256	3.21E-12	17.00482	26.96233

The equation comes out to be:

$$\frac{\tau_m}{\tau_0} = -14.70 - 7.31 \times P - 54.22 \times A^* + 21.98 \frac{V_{tip}}{V_{app}}$$

…….Eq.5.4

CHAPTER 6-CONCLUSIONS

6.1 Conclusions based on tip velocity

1. The difference in velocity ratio for tip velocity was observed according to permeability. The tip velocity increased from 1.25 times to the largest 1.7 times for the impermeable spur and the smallest 1.1 times for the permeable spur.

2. The tip velocity increases as the length of spur is increased for impermeable spur. For permeability upto 40%, tip velocity increases with increase in spur length. But for permeability greater than 60%, tip velocity remains same with increase in spur length.

3. The relative error of the tip velocity between experimental and numerical results is always less than 10%. The error becomes less as the approach velocity is increased.

4. A modified empirical equation for tip velocity and maximum velocity was developed using multiple linear regression.

6.2 Conclusions based on separation length

5. The separation length increases with the increase in spur length for same permeability. The separation length decreases with increase in permeability for same spur length.

6. The separation length was measured about 12.5 times the spur length for impermeable, 10 times the spur length for 20% permeable, 5.7 times the spur length for 40% permeable, 3 times the spur length for 60% permeable and 1.8 times the spur length for 80% permeable spur.

7. Recirculation zone is formed only in impermeable spur. There in nearly no velocity in the recirculation zone and the upstream part of impermeable spur. There was no recirculation zone formed in any of the permeable spur.

8. The relative error of the tip velocity between experimental and numerical results is always less than 5%.

6.3 Conclusions based on maximum bed shear stress

9. The bed shear stress was 7 times the undisturbed shear stress for impermeable spur. For permeable spur, it was around 3 times. So the impermeable spur has more potential of getting scoured.

10. An empirical equation for maximum bed shear stress was developed using multiple linear regression after knowing the values of tip velocity.

6.4 Overall conclusions

11. In case of impermeable spur, the velocity distributions in the recirculation zone and upstream part of spur have weak magnitude. These areas have considerable deposition. On the other hand, velocities of large magnitude can be observed around the foot of the spur due to convergence of flow and hence local scour occurs.

12. In case of permeable spur, the flow patterns present completely different behaviour compared to the impermeable spur. Local scour still occurs around the permeable spur but the magnitude of scouring is smaller than those in impermeable spur due to less bed shear stresses.

13. Hence permeable spur is better alternative than impermeable spur. Also the spur of 20% permeability gives the best results in the light of parameters such as separation length, tip velocities and bed shear stresses.

14. ANSYS Fluent gives good results when compared to the experimental results. So the numerical model can be substituted for the physical model and leads to cost and time savings in future design of spurs.

6.5 Future scope of study

In further studies the experiments related on the effect of installation angle, series of spurs, lateral slope of spurs, other shapes of spurs(T-type, L-type) can be done. Various models in ANSYS Fluent such as RANS model, LES model etc. can be used to analyse the flow around spurs.

REFERENCES

[1] Acharya, Anu, and Jennifer G. Duan. "Three dimensional simulation of flow field around series of spur dikes." *ASCE copyright Proceedings of the 2011 World Environmental and Water Resources Congress, California, USA*. 2011.

[2] Asayama, Chiharu."Study on Control for Suitable Bed Morphology around Successive Groynes".

[3] Baba, Y., et al. "Flows and bedload dynamics around spur dyke in a compound channel." *11th International Symposium on River Sedimentation (ISRS)*. 2010

[4] Duan, Jennifer G. "Mean flow and turbulence around a laboratory spur dike."*Journal of Hydraulic Engineering* (2009).

[5] Ettema, Robert, and Marian Muste. "Scale effects in flume experiments on flow around a spur dike in flatbed channel." *Journal of Hydraulic Engineering* (2004).

[6] Francis, J. R. D., A. B. Pattanaik, and S. H. Wearne. "Technical note.. Observations of flow patterns around some simplified groyne structures in channels." *ICE Proceedings*. Vol. 41. No. 4. Thomas Telford, 1968.

[7] Ghaldarbandi.R., M. H. Keshavarz, and H. Hakimzadeh. "Investigation of the Bed and Structural Slopes on Bed Shear Stress and Flow Characteristics around an Impermeable Groyne." *Journal of Hydraulic Structures* 1.1 (2013): 11-23

[8] Ghani, Usman, Shahid Ali, and Sabhat Arif. "Influence of Spur Dike on Flow Patterns in an Open Channel."

[9] Hakimzadeh, H., Azari, N. and Mehrzad, R. "Experimental Study of the Effect of Lateral Structural Slopes of Groynes on Scour Reduction", Proceedings of Sixth International Conference on Scour and Erosion, Paris, France, 2012.

[10] Handbook for Flood protection, anti erosion and river training works, Central water commission, New Delhi

[11] Ho, Jungseok, et al. "Numerical modeling study for flow pattern changes induced by single groyne." *Proceedings of the Congress-international Association for Hydraulic Research*. Vol. 32. No.2.2007

[12] Kafle, Mukesh Raj. "Numerical Simulation of Flow around a Spur Dike with Free Surface Flow in Fixed Flat Bed." *Journal of the Institute of Engineering* 9.1 (2014): 107-114.

[13] Kang, Joongu, et al. "Experimental investigation on the local scour characteristics around groynes using a hydraulic model." *Water and Environment Journal* 25.2 (2011): 181-191

[14] Karami, Hojat, et al. "Verification of numerical study of scour around spur dikes using experimental data." *Water and Environment Journal* 28.1 (2014): 124-134

[15] Mansoori, Amir-Reza, et al. "Three-Dimensional Features of the Turbulent Flow around Series of Groynes with Different Shapes of Head." *Journal of Japan Society of Civil Engineers, Ser. B1 (Hydraulic Engineering)* 68.4 (2012): I_61-I_66.

[16] McCoy, Andrew, George Constantinescu, and Larry J. Weber. "Numerical investigation of flow hydrodynamics in a channel with a series of groynes."*Journal of Hydraulic Engineering* 134.2 (2008): 157-172.

[17] Mioduszewski, Tomasz, Shiro Maeno, and Yatsugi Uema. "Influence of the spur dike permeability on flow and scouring during a surge pass." *International Conference on Estuaries and Coasts*. 2003.

[18] Ouillon, Sylvain, and Denis Dartus. "Three-dimensional computation of flow around groyne." *Journal of hydraulic Engineering* 123.11 (1997): 962-970.

[19] Rajaratnam, Nallamuthu, and Benjamin A. Nwachukwu. "Flow near groin-like structures." *Journal of Hydraulic Engineering* 109.3 (1983): 463-480.

[20] Safarzadeh, A., et al. "Experimental study of head shape effects on shear stress distribution around a single groyne." *River flow 2010, Proceedings of 5th International Conference on Fluvial Hydraulics*. 2010.

[21] Shahrokhi, Mahdi, and Hamed Sarveram. "Three-dimensional simulation of flow around a groyne with large-eddy turbulence model." *Journal of Food, Agriculture & Environment* 9.3&4 (2011): 677-681.

[22] Shamloo, Hamid, and Bahareh Pirzadeh. "Numerical Simulation of the Angle of Groyne Installation on the Separation Zone Length Behind it." *Journal of River Engineering* 2 (2014).

[23] Tang, Xuelin, Xiang Ding, and Zhicong Chen. "Large eddy simulations of three-dimensional flows around a spur dike." *Tsinghua Science & Technology* 11.1 (2006): 117-123.

[24] Tingsanchali, Tawatchai, and Selvaratnam Maheswaran. "2-D depth-averaged flow computation near groyne." *Journal of Hydraulic Engineering* 116.1 (1990): 71-86.

[25] Uijttewaal, Wim S. "Effects of groyne layout on the flow in groyne fields: Laboratory experiments." *Journal of Hydraulic Engineering* (2005).

[26] Yazdi, J., et al. "3D simulation of flow around a single spur dike with free-surface flow." *Intl. J. River Basin Management* 8.1 (2010): 55-62.

[27] Yeo, Hong Koo, Joon Gu Kang, and Sung Jung Kim. "An experimental study on tip velocity and downstream recirculation zone of single groynes of permeability change." *KSCE Journal of Civil Engineering* 9.1 (2005): 29-38.

[28] Yossef, Mohamed FM, and Huib J. de Vriend. "Flow details near river groynes: experimental investigation." *Journal of Hydraulic Engineering* 137.5 (2010): 504-516.

[29] Yossef, Mohamed FM. "The effect of groynes on rivers." *Literature Review*(2002).

[30] Yossef, Mohamed Fathy Mohamed. *Morphodynamics of rivers with groynes*. TU Delft, Delft University of Technology, 2005.

[31] Zhang, Hao, et al. "Experiment Study on Channel Bed Characteristics around Spur Dykes of Different Shapes." *Journal of Japan Society of Civil Engineers, Ser. A2 (Applied Mechanics (AM))* 69.2 (2013): I_489-I_499.